Ph. D. Dissertation

Tracing the evolution of multiscale functional network and prediction of spontaneous remission in the EEG of depression mouse models using persistent homology

Persistent Homology 를 이용한 우울증 쥐 모델 뇌전도에서의 자발적 회복 예측과 다중축적 기능적 네트워크 발달 추적에 관한 연구

Arshi Khalid

Department of Bio and Brain Engineering

KAIST

2015

Tracing the evolution of multiscale functional network and prediction of spontaneous remission in the EEG of depression mouse models using persistent homology

Persistent Homology 를 이용한 우울증 쥐 모델 뇌전도에서의 자발적 회복 예측과 다중축적 기능적 네트워크 발달 추적에 관한 연구

Tracing the evolution of multiscale functional network and prediction of spontaneous remission in the EEG of depression mouse models using persistent homology

Advisor : Professor Jong Chul Ye

by

Arshi Khalid

Department of Bio & Brain Engineering

KAIST

A thesis submitted to the faculty of KAIST in partial fulfillment of the requirements for the degree of Doctor of Philosophy in the Department of Bio & Brain Engineering. The study was conducted in accordance with Code of Research Ethics[1]

2014. 10. 06

Approved by

Professor Jong Chul Ye

[Advisor]

[1]Declaration of Ethical Conduct in Research**:** I, as a graduate student of KAIST, hereby declare that I have not committed any acts that may damage the credibility of my research. These include, but are not limited to: falsification, thesis written by someone else, distortion of research findings or plagiarism. I affirm that my thesis contains honest conclusions based on my own careful research under the guidance of my thesis advisor.

Tracing the evolution of multiscale functional network and prediction of spontaneous remission in the EEG of depression mouse models using persistent homology

Arshi Khalid

The present dissertation has been approved by the dissertation committee as a PhD dissertation committee at the KAIST

October 06, 2014

Committee head: Prof. Ye Jong Chul

Committee members: Prof. Jeong Yong

Prof. Jeong Jaeseung

Prof. Paik Se-Bum

Prof. Jeong Bumseok

DBIS

20115358

아르쉬 칼리드. Arshi Khalid. Tracing the evolution of multiscale functional network and prediction of spontaneous remission in the EEG of depression mouse models using persistent homology. Persistent Homology를 이용한 우울증 쥐 모델 뇌전도에서의 자발적 회복 예측과 다중축적 기능적 네트워크 발달 추적에 관한 연구. Department of Bio & Brain Engineering. 2015. 51p. Advisor Prof. Jong Chul Ye. Text in English.

ABSTRACT

Many brain diseases or disorders such as depression have known to have a manifestation with abnormal functional connectivity in neural networks of the brain. To explore heterogeneous depressive symptom domains, it is unlike to get it explained by the functional connectivity with just conventional bivariate measures for coupling analysis such as cross correlation and coherence. We adopted an inclusive approach by investigating depression mouse model EEG at neuronal network level, ensuring the optimal use of the wealth of the information present in the data. For geometrical exploitation of the brain network evolution, we here applied persistent brain network homology analysis to EEG signals from a mouse model of depression. The EEG signals were obtained from eight different cortical regions (frontal, somatosensory, parietal, and visual cortices at each hemisphere). The persistent homology revealed the significantly altered functional connectivity between the control and depression mouse model, which was not appeared in the common coupling measures such as cross correlation and coherence. Depression mouse model showed more localized connectivity and decreased global connectivity compared to the control. Particularly, somatosensory and parietal cortices are loosely connected in the depression model. In addition, the depression model displayed altered connections among the cortical regions, especially between the frontal and somatosensory cortices, compared to the control. This study provides that persistent homology is useful for the brain network analysis, and our results demonstrate that depression animal brain shows more localized connectivity and decreased global connectivity with altered connections, which can help to characterize abnormal brain network underlying depression.Further, many ailments including depression are self-limiting and improve with time irrespective of treatment and this change is termed as spontaneous remission. Recently,

restitution factors for depression has explored and checked for the relevance with EEG quantitative analysis for prediction. In this study, we investigated EEG-alert state data from chronic restrain stress (CRS) induced mouse models. After three weeks which is the perceived time course for spontaneous recovery in depression, again these models underwent EEG recordings. We found restored cortical spectral power after three weeks in the CRS model when compared to the control group. Frontal and somatosensory cortices mainly showed spontaneous recovery. Network level functional connectivity was analyzed using persistent brain network homology along with other graph theoretical measures. It was revealed that the altered functioning of temporal oscillations on a network level after three weeks was similar to the control group mainly involving somatosensory cortices with other regions at gamma frequency range (31-80 Hz). Which may present gamma oscillations of cortical regions as predictor in the recovery of affected brain from depression.

Keywords: Persistent brain network homology, EEG, Functional connectivity, Depression, Spontaneous remission, Biomarker

Table of Contents

List of figures

Chapter 1 . Introduction

Depression is one of the most prevalent mood disorders and is characterized by diverse symptoms including sad mood, loss of interest, and unhappiness and high comorbidity with other brain dysfunctions [1-4]. Epidemiological studies reported that depression is common across the lifespan with 20% of the population worldwide experiencing a depressive episode during their lifetime, and 2-5% of the population are affected by severe depression [5, 6]. Depression is unlikely to stem from aberrant function of a specific gene or brain region [7]. Many studies have reported that numerous regions of the brain are affected by depression[8], and that the symptoms of depression are associated with the dysregulation of a distributed neural networks encompassing cortical regions rather than the functional breakdown of a single discrete brain region [7-13]. Therefore, in order to explain in depth the heterogeneous domains of depression's symptoms, it is critical to implement a method that analyzes the global functional networks rather than a single region or a local circuit.

In the endeavor towards a better understanding of the human brain's functioning, the analysis of task-dependent information transfer between brain regions plays a crucial role. An intermediate step towards unified brain modeling is models that describe the dynamics and interaction patterns of brain regions on a macroscopic scale. This is the strategy pursued by the majority of studies in brain connectivity analysis. There exist various competing definitions of "connectivity" and there is an even greater disagreement on how to properly measure connectivity according to the various definitions. Regarding the first point, a distinction between structural, functional and effective connectivity has been widely agreed on [14-16]. Structural connectivity refers to the static anatomical structure of the brain, which can be acquired, for example, by a single scan using a high-resolution anatomical MRI [17] or diffusion tensor imaging (DTI,[18]) device. Functional and effective connectivity are defined with respect to a mental task and refer to "coupled" activity of two neuroanatomical entities during task execution. The common distinction between the two is that effective connectivity is directed, i.e., describes a driver-receiver relationship, while functional connectivity is not. Originally, functional connectivity had been equated with instantaneous correlation [16] but it is useful to extend this definition to arbitrary measures of

undirected functional dependencies which are symmetric in their arguments. Analogously, effective connectivity might be quantified by any asymmetric function. There is an infinite number of functions complying with these definitions and indeed, the applied connectivity measures are numerous and originate from diverse fields such as graph theory, signal processing and Persistent Homology. Here, we are primarily concerned with measures of functional and effective connectivity based on persistent brain network homology and partial directed coherence respectively.

Functional connectivity, which is defined as the temporal correlation between spatially remote neurophysiological events [19], is believed to serve as the mechanism for the coordination (or discoordination) of activity between different neural populations or systems across the cortex [20, 21].

According to recent interpretations of large-scale neural interactions, functional connectivity between the distributed events across the neural networks is very critical for particular brain works [22, 23]. Electroencephalographic (EEG) signals have been used for the analysis of the functional connectivity in patients with depression [24-30]. The EEG coherence analysis is one of the most widely used approach for measuring functional connectivity in the coupled neural systems. However, coherence analysis may result in; increase, decrease, or even no change in functional connectivity in the depression brain [27, 30]. One potential explanation for this varied/unstable result is that coherence determines only the linear characteristics of the EEG time series and can detect with particular sensitivity profile [30, 31]. Cross-correlation analysis is also widely used for measuring functional connectivity in the coupled neural systems. In the correlation approaches to construct brain connectivity map, the coupling strengths are decided depending upon the optimal threshold level. The issue with these standard methods is that there are no generally accepted criteria for determining the proper threshold [32], thus some of the functional connections cannot easily come out (hidden connectivity). To obtain the proper threshold, the multiple-comparison correction over every possible connection could be applicable. However depending on what *p*-value to threshold, the resulting connectome also changes [33-36]. Thus, it is necessary for an inclusive approach to ensure the optimal use of the wealth of the information present in the EEG signals, which can give accurate and elaborate functional dynamics that underlie the mechanism of depression-related symptomatic manifestation.

Very recently, a multiscale hierarchical network modeling framework that surpass the limitation (i.e., the problem of determining one optimal threshold) and traces the evolution of network changes over different thresholds was developed [32]. This concept is persistent brain network homology; it handles and analyzes multiscale networks by identifying the persistent topological features over the changing scales. With application of the persistent brain network homology into the signals from FDG-PET of attention-deficit hyperactivity disorder, the study could elaborate functional brain connectivity [30, 32].

Though not without limitations, the use of animal models do play an important role in the understanding of human brain's pathophysiological mechanisms [37]. For instance, the chronic exogenous exposure to corticosterone (CORT) via drinking water has been used frequently to induce human depression-like behavior, neurochemistry, and brain morphology in mice [38, 39]. Furthermore, unlike the clinical data where the depression is diagnosed based on somewhat subjective criterion, animal model is very useful for studying brain connection changes from depression systematically since we can easily control the pathology objectively. Therefore, in this study, we intensively investigated the functional connectivity by applying the persistent brain network homology to EEG data from eight different cortical regions (frontal, somatosensory, parietal, and visual cortices at each hemisphere) of a CORT-induced mouse model of depression. The hidden brain network in the pathological brain of depression was successfully revealed by the persistent brain network homology technique. We present the compelling evidence about the compromised functioning of cortical circuitry and the aberrant functional connectivity in the affective illnesses of depression.

Chapter 2 . Multiscale functional networks in corticosterone induced depression mouse model using persistent brain network homology

2.1 Generation of the depression model

Adult male C57BL/6 mice (7~8-week-old) were used. The animal model of depression was generated by chronic exposure to corticosterone (CORT) as described previously [39]. 35 ug/ml CORT (Sigma, St. Louis, MO) was dissolved in drinking water with 0.45% β-Cyclodextrin (β-CD) (Sigma, St. Louis, MO) for the mouse (CORT group). CORT was delivered in light-protected bottles, and was replaced every 3 day for up to 28 days. Control mice received β-CD only (vehicle, VEH group). Mice were housed under a 12-h light/dark cycle and had ad libitum access to food and water. Animal care and handling were carried out according to the guidelines approved by the Institutional Animal Care and Use Committee at the Korea Advanced Institute of Science and Technology (KAIST).

2.2 Behavioral tasks

The depressive phenotype of CORT group was verified with some behavioral tasks: Forced swim task for despair behavior, Elevated plus maze for anxiety, Open field test for locomotion (Fig.1), and the results were similar with those of the previous reports [38, 39]. Behavioral experiments were performed after the CORT or vehicle treatment. Behavioral tests were conducted between 4PM and 8PM at the light intensity of 80 lux, and performed as described previously [40, 41]

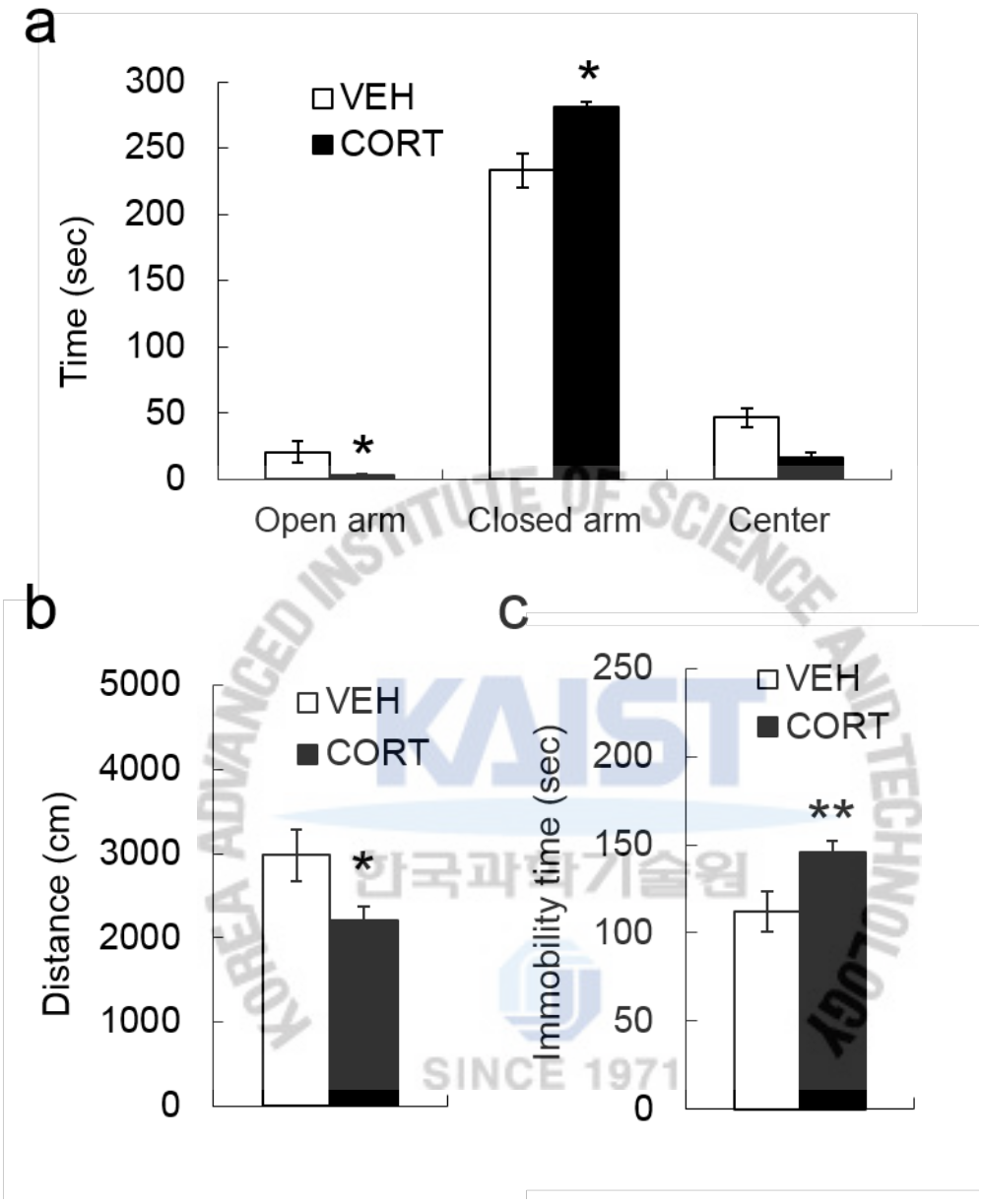

Figure 2.1: Behavioral phenotypes of depression in the CORT group. (a) Elevated plus maze. The CORT group (n = 9) spent less time in the open arm and more time in closed arm compared to the VEH group (n = 7), indicating a high level of anxiety in the CORT group. (b) Open field test. The CORT group (n = 11) moved a lesser distance than the VEH group (n =8) did, which indicate reduced locomotor activity of the CORT group. (c) Forced swim task. The CORT group (n = 11) showed increased immobility compared with the VEH group (n = 10), indicating a higher level of despair behavior in the CORT group. * $p < 0.05$, ** $p < 0.01$, Student's t-test.

2.3 Electrode implantation and in vivo electrophysiology for EEG

Animals underwent EEG surgery immediately after the CORT or vehicle treatment. Animals were anesthetized by intraperitoneal injection of ketamine (90 mg/kg) and xylazine hydrochloride (40 mg/kg). Electrode implantation was performed with a stereotaxic apparatus (Kopf Instruments, Tujunga, CA, USA). EEG recordings were obtained with tungsten electrodes (0.005 in., 2 MΩ), which were positioned in eight different cortical regions based on a mouse brain atlas [42]: frontal cortices (AP +1.5 mm, L ±0.2 mm, and DV –1.0 to –1.1 mm), somatosensory cortices (AP 0.0 mm, L ±1.5 mm, and DV –1.0 to –1.1 mm), parietal cortices (AP -2.0 mm, L ±2.5 mm, and DV –1.0 to –1.1 mm), and visual cortices (AP -3.5 mm, L ±1.5 mm, and DV –1.0 to –1.1 mm) at each hemisphere (depicted in Fig. 2.2(a)). A reference electrode was inserted on the skull over the cerebellum. The electrodes were fixed to the skull with cyanoacrylate and dental acrylic cement. EEG recordings were combined with video monitoring, and the EEG-video recording data were continuously obtained 24 h per day for at least 5 days. EEG activity was recorded after the signal was amplified to 1200-fold, bandpass-filtered at 0.1 to 70 Hz, and digitized with a sampling rate of 400-Hz using a digital EEG system (Comet XL, Astro-Med, West Warwick, RI, USA). The obtained EEG-video data was analyzed offline using PSG Twin (Astro-Med, West Warwick, RI, USA), Clampfit (Axon Instruments, Foster City, CA, USA), and Matlab (MathWorks, Natick, MA, USA).

2.4 Persistent Brain Network Homology

Continuous EEG signals from the animals for three epochs, each consisting of 1 min of data from different days, in which they were in a resting state (i.e., awake and no movement), were analyzed to check the stability of the findings. Then, continuous 1-min-long EEG signals from the last day of recording were used for analyses (Fig. 2.2). The five EEG frequency-bands—delta (1.5-4Hz), theta (4-8Hz), alpha (8-12Hz), beta (12-30Hz), and gamma (30-60Hz)—were analyzed using a persistent brain network homology approach for functional connectivity.

EEG measurements were obtained in the eight selected ROIs (left frontal cortex, right frontal cortex, left somatosensory cortex, right somatosensory cortex, left parietal cortex, right parietal cortex, left visual cortex, right visual cortex) in ten control mice (β-CD vehicle, VEH group) and nine CORT-drinking mouse models of depression-like behavior (corticosterone, CORT group).

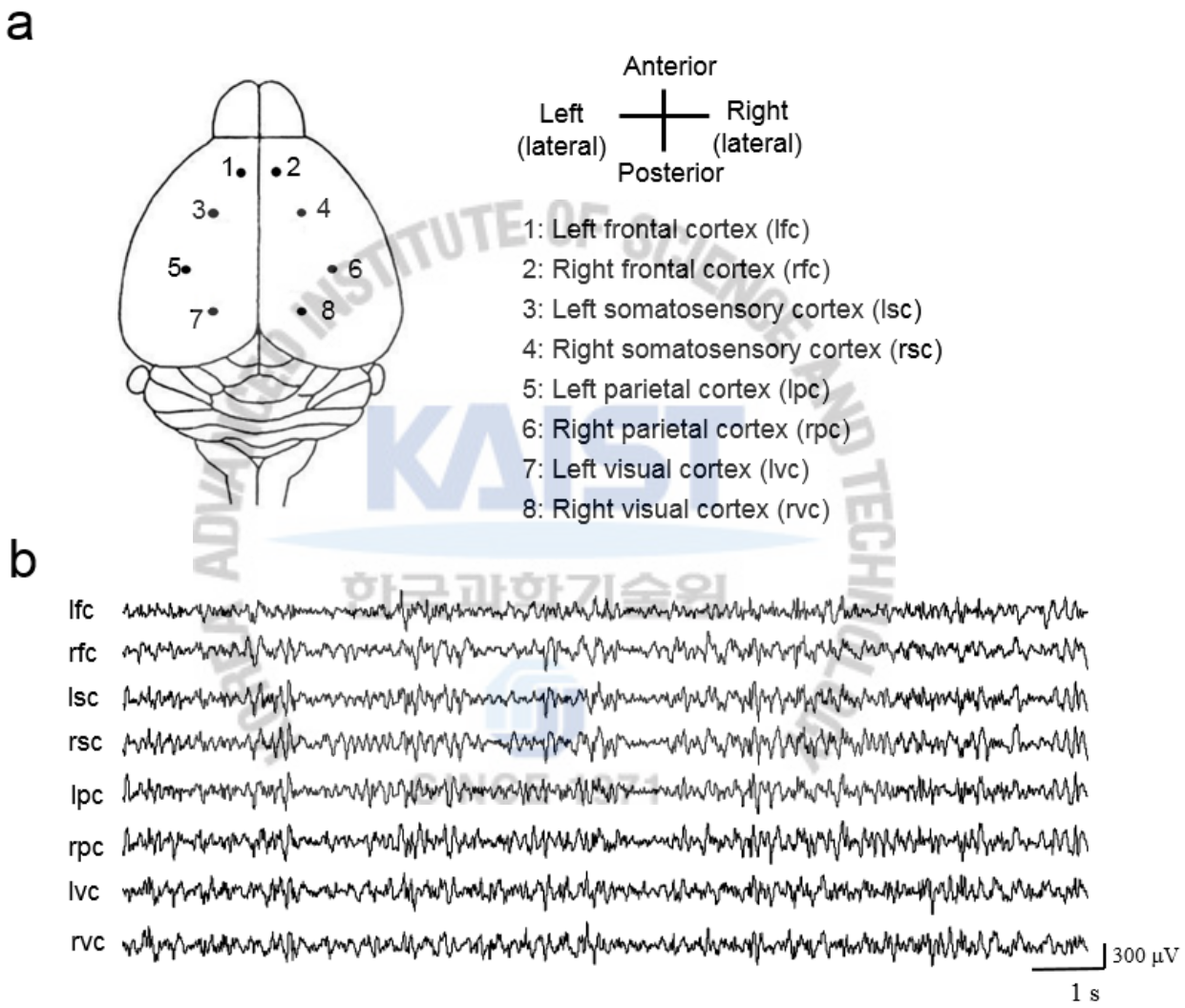

Figure 2.2: A schematic drawing for electrode position and EEG signals. (a) Drawing of top view mouse brain depicting electrode positions and names of the regions/nodes. (b) Representative original traces of electroencephalogram (EEG) recordings in the 8 different cortical regions; lfc (left frontal cortex)s, rfc (right frontal cortex), lsc (left somatosensory cortex), rsc (right

somatosensory cortex), lpc (left parietal cortex), rpc (right parietal cortex), lvc (left visual cortex), rvc (right visual cortex) in order.

The measurement set was denoted as M = {m_1, m_2,…, m_8}consisting of eight nodes (i.e., the eight brain regions) where we had measured m_i at the i^{th} node. We calculated the distance matrix c_M between two EEG measurements m_i and m_j, using the following equation:

$$c_M(m_i, m_j) = \sqrt{1 - corr(m_i, m_j)}. \quad (1)$$

where $corr(m_i, m_j) = \left\langle \frac{m_i}{\|m_i\|}, \frac{m_j}{\|m_j\|} \right\rangle$ refers the sample correlation between m_i and m_j. Thus, we used the square root of (1-correlation) distance metric to construct binary network.

The brain network can be viewed as a weighted graph (M, c_M) where M is a set of measurements at each brain region (= node) and c_M is the metric defined on that set. We connect the nodes i and j with an edge if the distance $c_M(m_i, m_j) \leq \varepsilon$ for some threshold value, ε. Then, the *binary network* B(M,ε) at threshold ε is a graph consisting of the nodes and the edges as depicted in Figure 2.3(b). The binary network B(M, ε) consists of 0-simplices (nodes) and 1-simplices (edges).

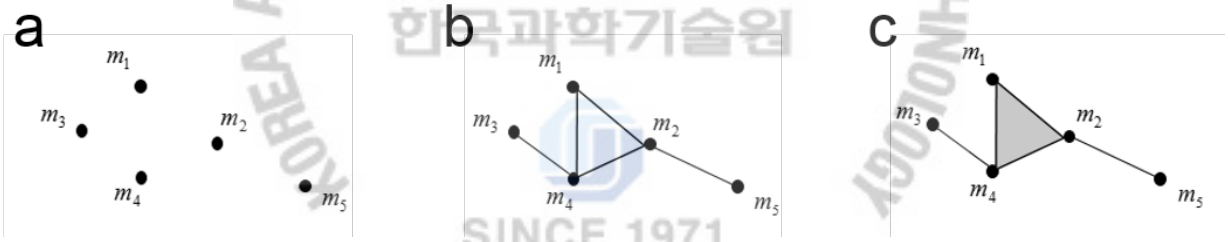

Figure 2.3: The Schematic draw of binary networks and Rips complex. (a) Cluster of p (=5) data points considered to be as nodes or ROIs in the brain network study. (b) The Binary network of set M= {m_1, m_2, … , m_p}, points got connected given some criteria on distance. (c) The Rips complex: including faces as well.

Previous studies on brain network modeling used a single fixed threshold, ε, whereas persistent brain network homology is a novel multi-scale hierarchical network modeling framework that traces the evolution of network changes over different thresholds [32], starting with ε = 0 and increasing ε at each iteration. The value of ε is taken discretely from the smallest $c_M(m_i, m_j)$ to the largest $c_M(m_i, m_j)$. By increasing ε, more connected edges may become involved. If two nodes are

already connected, directly or indirectly, via other intermediate nodes with a smaller ε then at a larger ε they will not be connected. When ε is larger than any distance $c_M(m_i, m_j)$, the iteration terminates because the graph does not change further. Suppose G_k is the graph obtained at the k^{th} iteration with $\varepsilon = \varepsilon_k$. Then, upon changing the threshold, for $\varepsilon_0 \leq \varepsilon_1 \leq \ldots \leq \varepsilon_n$, we obtain a sequence of graphs that correspond to binary networks $B(M,\varepsilon_0)$, $B(M,\varepsilon_1)$, $B(M,\varepsilon_2)$,…. Furthermore, the sequence of graphs follow a hierarchy $G_1 \subset G_2 \subset G_3 \subset \ldots$. Such a sequence of nested graphs is termed a graph filtration in algebraic topology.

More specifically, given a point cloud data M, the *Rips complex* $R(M,\varepsilon)$ is a simplicial complex whose k-simplices correspond to unordered (k+1)-tuples of points that are pair-wise within distance ε. Given a point cloud data set consisting of p nodes (i.e., the number of nodes), the Rips complex has at most (p-1) simplices whereas a binary network has at most 1 simplex (see Figure 2.3). The Rips complex can also have faces. When ε increases, the subsequent Rips complex becomes larger than all previous Rips complexes. Thus, we have $R(M, \varepsilon_0) \subseteq R(M, \varepsilon_1) \subseteq \ldots \subseteq R(M, \varepsilon_n)$ for $\varepsilon_0 \leq \varepsilon_1 \leq \ldots \leq \varepsilon_n$. The nested sequence of the Rips complex is known as a *Rips filtration,* which is a major theme in persistent homology. A binary network is a subset of the Rips complex [32]. Thus, we can have a graph filtration for the case of binary networks as $B(M, \varepsilon_0) \subseteq B(M, \varepsilon_1) \subseteq \ldots \subseteq B(M, \varepsilon_n)$.

As shown in Figure 2.4(a), as the filtration value, ε, changes, the topological characteristics of the binary network change. The topological change in the filtration can be visualized using the barcode, constructed by plotting the changing topological features over different filtration values. The topological feature is displayed using a bar that starts and ends when the feature appears and disappears. The barcode represents the changes in topological features when the filtration value changes. Among the many topological features, here, the zeroth Betti number, which counts the number of connected components in a network, is our interest. Because the p^{th} Betti number is estimated by the p- and (p+1)-simplices, the binary network B(M, ε) contains enough information to compute β_0. In Figure 2.4 (b), we plotted the zeroth Betti number β_0 (vertical axis) of the Rips complex over the filtration values $\varepsilon_0, \varepsilon_1, \ldots, \varepsilon_n$ (horizontal axis).

Other brain network studies, such as characteristic path length, clustering coefficients, assortativity, and modularity, focus on reflecting different topological characteristic of the brain network and measuring similarities between them. These measures quantify the network properties

after all nodes are connected. However, the change in β_0 shows topological changes in a network before all nodes are connected.

While the barcode in Figure 2.4 (b) represents global topological changes in a network, rearranging the bars in the barcode and connecting the bars according to the node index and the Rips filtration, we obtain a single-linkage dendrogram (SLD) Figure 2.4 (c).

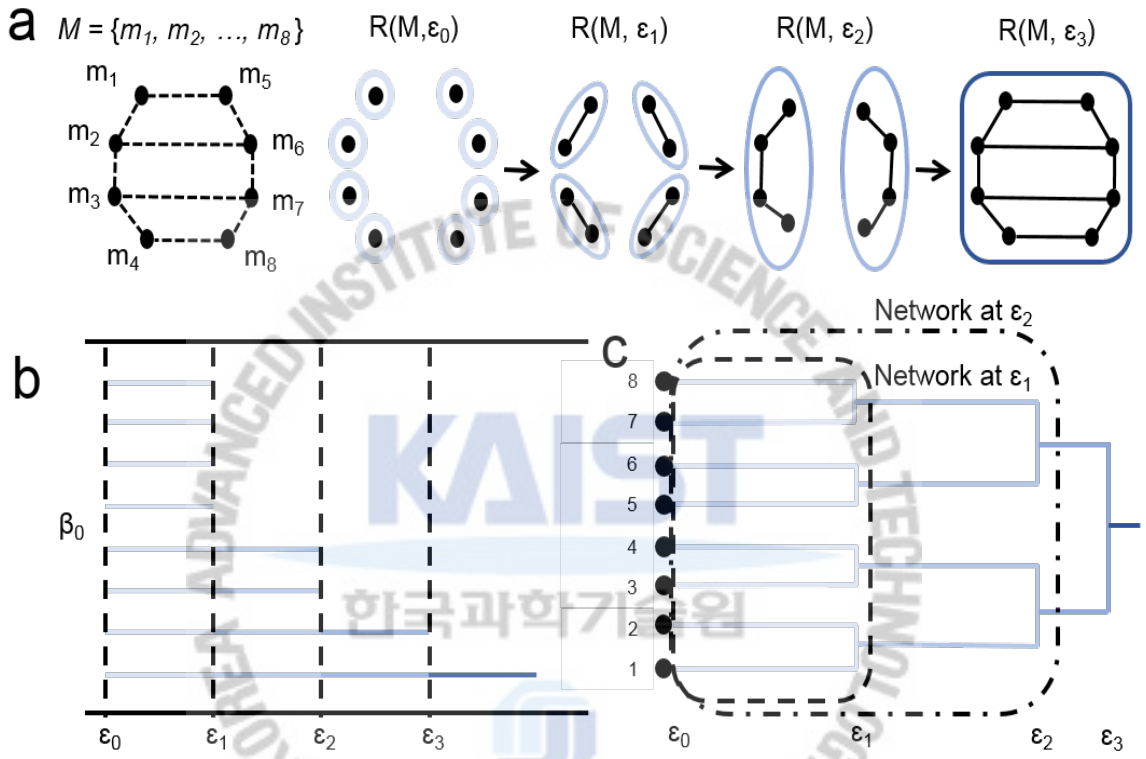

Figure 2.4: The schematic draw of the network evolution over increasing filtration values ε0, ε1, ε2, and ε3. (a) Node set M and the Rips filtration at the filtration values ε_0, ε_1, ε_2, and ε_3 (b) barcode exhibits the changing topological features. The y-axis is zeroth Betti number (counts the number of connected components) while filtration values are along x-axis. (c) Single linkage dendrogram SLD depicting geometrical information of subnetworks formation before merging into one big connected component.

Consider the Rips filtration. Let C_m^k and C_n^k be the two disconnected components of the Rips complex R(M, ε_k). Suppose there exist two nodes m_i in C_m^k and m_j in C_n^k such that the distance d

between them is less than the next filtration value ε_{k+1}. Then, these two disconnected components will be connected at ε_{k+1} if

$$d(C_m^k, C_n^k) = \min \min_{x_i \in C_m^k, x_j \in C_n^k} d(x_i, x_j) < \varepsilon_{k+1}$$

The sequence of merged components during the Rips filtration is identical to the sequence of the merging in dendrogram construction [32]. The linking of two nodes corresponds to merging two leaves in the dendrogram.

Regardless of which node we start with, a consistent dendrogram is always generated. In Figure 2.4 (c), the SLD shows the local network characteristics of the subnetworks that are clustered together at earlier filtration values before merging into one large component. Using SLD, we can recompute the distance between the nodes in the network using the single-linkage distance, a model predictive distance using SLD. Mathematically the single-linkage distance is given by:

$$d_M(m_i, m_j) = \min\{\max_{l=0,\cdots,k-1} c_M(w_l, w_{l+1}) / m_i = w_0, \cdots, w_k = m_j\} \quad (2)$$

where $m_i = w_0, \ldots, w_k = m_j$ is a path between m_i and m_j.

2.4.1 Statistical Analysis

For intergroup comparisons of behaviors, Student's *t*-test was used, and all data for behaviors are presented as means ± standard error of mean (SEM). A P-value < 0.05 was considered to indicate statistical significance. The Mann-Whitney U-test and the Wilcoxon rank-sum test were used for intergroup comparisons of EEG data. The SPSS software (ver. 21.0; SPSS Inc., Chicago, IL) and Matlab were used for statistical analyses.

For the calculation of p-values of slopes and final filtration values in the barcode, we resampled the correlation matrix of each subject using bootstrapping (1000 replications), and obtained the slopes and final filtration values of the barcode based on resampled data sets. Then, the Wilcoxon rank-sum test was performed for the statistical comparison of slopes and final filtration values of the barcodes between the groups. The Mann-Whitney-Wilcoxon test was used to compare pair-wise single-linkage matrices with a Bonferroni correction.

2.5 Results

We computed correlation-based distance matrices c_M (1) for the CORT and VEH groups (Fig. 2.5). Each ijth entry in the distance matrix is a correlation-based functional distance between two nodes m_i and m_j, calculated with equation (1). Visually, neither group displayed a clear separation of clusters arising from regional couplings (Fig. 2.5, 2.6).

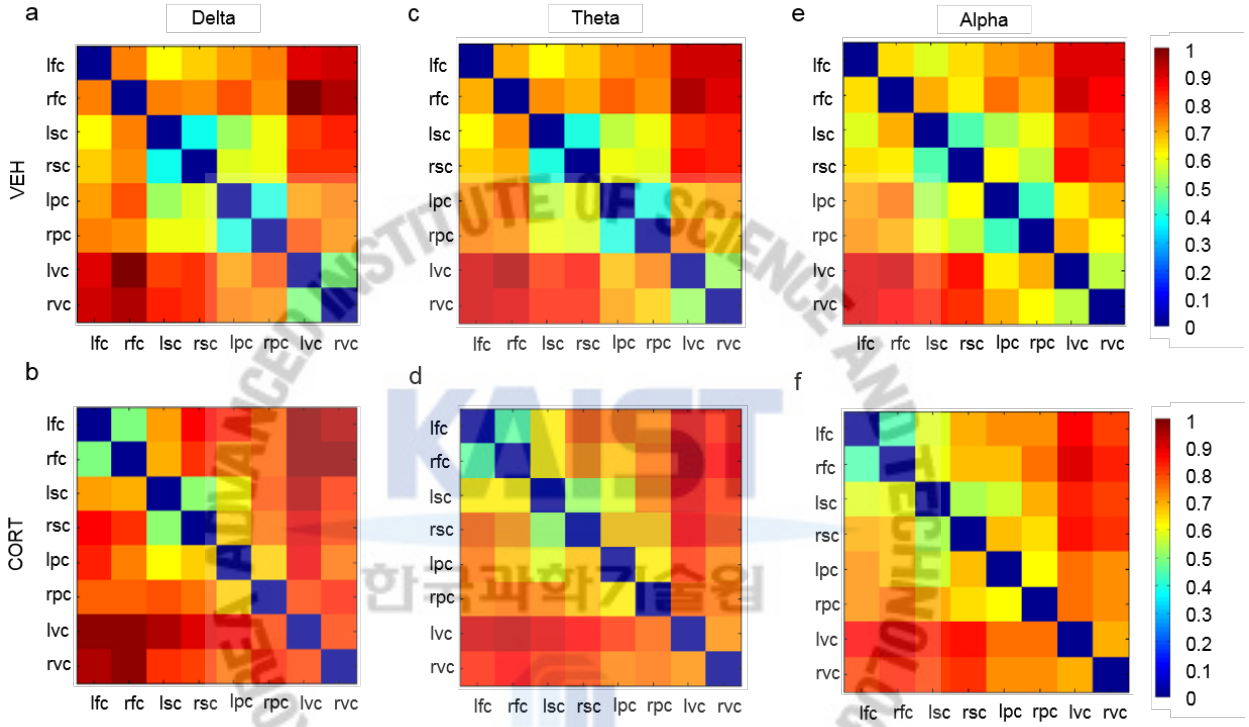

Figure 2.5: Distance matrices depicting statistical dependencies. Correlation-based distance matrices at delta-, theta-, and alpha-frequency bands in the VEH (a, c, and e) and CORT groups (b, d, and f). The distance matrices visually provide inefficient information on the ascertain group differences.

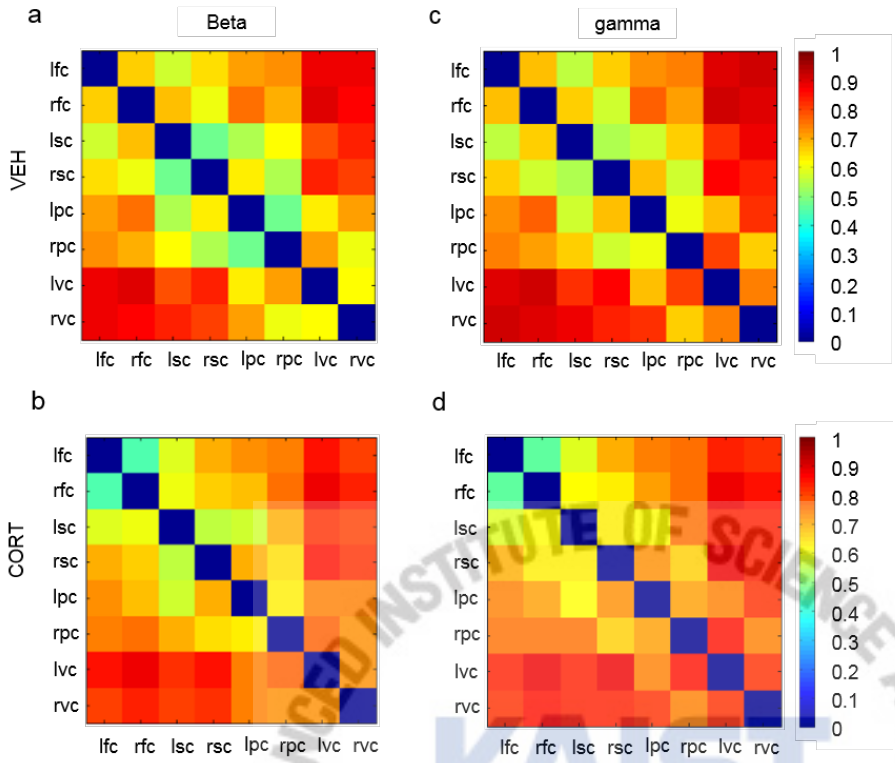

Figure 2.6: Distance matrices depicting statistical dependencies. Correlation-based distance matrices at beta- and gamma-frequency bands in the VEH (a, c) and CORT groups (b, d).

Next, we applied the persistent homology approach to explore functional connectivity at the network level for each frequency band of the EEG data recorded from the CORT and VEH groups. We obtained the persistent topological features in the brain network, changing over increasing filtration values using barcodes. Filtration was performed between 0 and 1 because all of the brain regions or nodes merged together before filtration reached 1, eliminating the need to consider distance values larger than 1. Based on the barcodes, we also constructed connectivity maps to incorporate the geometrical information about the positions of the connected nodes (the eight brain regions). Furthermore, we computed single-linkage distance matrices and the dendrogram for the predicted distances between the eight nodes and for the single-linkage hierarchical clustering, respectively.

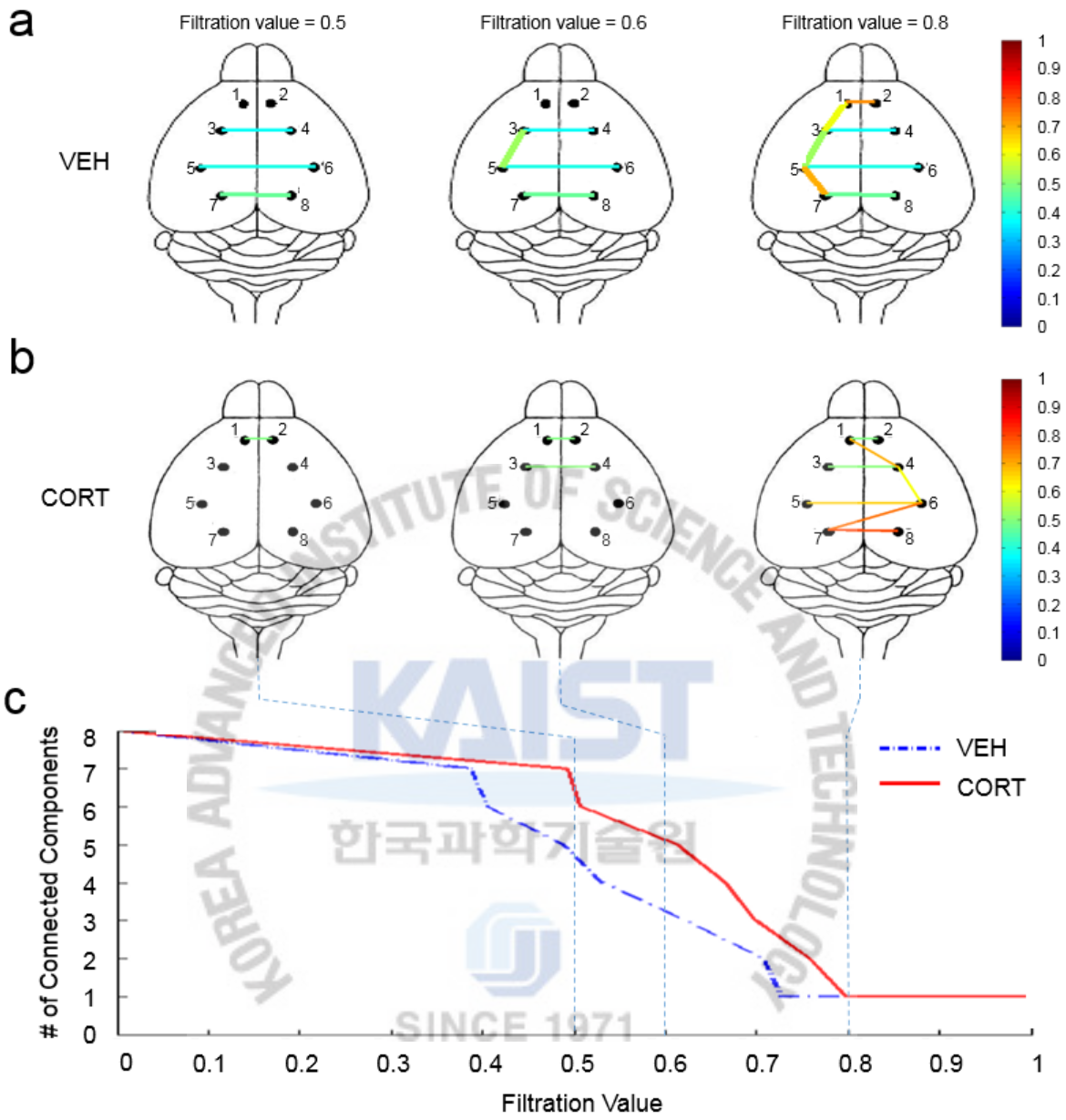

Figure 2.7: Trace of network evolution over changing filtration values at the delta-frequency band. Connectivity maps of the VEH (a) and CORT (b) groups at the filtration values ε=0.5, 0.6, 0.8, where color strength in the colorbar represents the functional distance between the nodes. The altered and decreased functional connectivity in the CORT group is shown in the brain network connectivity map. The overlaid barcodes of the VEH and CORT groups are showing brain network evolution over the different filtration values in (c) where final filtration value of the CORT group (= 0.7979) > the VEH group (=0.7281) at 95% level of confidence with Wilcoxon rank-sum test

of resampled datasets. Thus the CORT group with longer heavy tail is exhibiting decreased global connectivity with 95% level of confidence.

Figure 2.6(a-c) shows the connectivity map and barcode at the delta-frequency band for the VEH and CORT groups. In Figure 2.6(c), the overlaid barcodes are presented for the intergroup comparison between the VEH and CORT groups. The CORT group showed an increased number of connected components (zeroth Betti number, β_0) at filtration values from 0.4 to 0.8 in the barcode versus the VEH group. The maximum single-linkage distances (i.e., the final filtration value) of the VEH and CORT groups were 0.7281 and 0.7979, respectively. The final filtration value for the two groups were CORT > VEH at 95% level of confidence (tested with the Wilcoxon rank-sum test for resampled datasets, when resampling was performed using a bootstrap approach). These results indicate decreased global connectivity in the CORT group. Taken together, the higher β_0 with changing filtration values and the longer heavy tail in the shape of the barcode of the CORT group indicate more localized and decreased global connectivity. Moreover, the decreasing slopes of the barcodes were slope CORT (= 18.1871) > slope VEH (= 15.6128), with a significance level 0.05 (Wilcoxon rank-sum test for resampled data sets). Here, interpretation of local connectivity should not be confused with the criteria for reading the barcode graph for global connectivity, which is how a large subnetwork is reached at an earlier threshold. Local connectivity is an indicator of how many local connected clusters there are at a particular filtration value. For example, the VEH group had four local clusters of connected components at a filtration value of 0.6. However, the CORT group had six local clusters of connected components at the same value (Fig. 2.6), indicating more localized connectivity. The connectivity maps at three different values (ε = 0.5, 0.6, 0.8) from the barcodes are shown in Figure 2.6[43]. The color of the color bar is simply a filtration value, serving as an edge weight between two connected nodes. A lower filtration value, or a cooler color indicates increased connectivity and less functional distance, whereas a high filtration (anti-correlation) value indicates decreased connectivity and a higher functional distance. The altered connectivity pathways of the CORT group can be visualized readily using geometrical maps. The decreased connectivity at each filtration value indicates hypoactivation of the final network in the CORT group.

Figure 2.7[43] shows a single-linkage matrix for the delta-frequency band of the VEH and CORT groups, illustrating the functional distance between the brain regions. This single-linkage matrix could produce efficient separation of the brain subnetworks within each group, compared with the correlation-based distance matrices shown in Figure 2.5. Each $_{ij^{th}}$ entry in the single-linkage matrix is a model-based predicted functional distance between the two nodes, m_i and m_j. The Mann-Whitney test for exact probabilities was used to assess the difference in subnetworks between the groups. The model-predicted distances from single-linkage matrices were tested with the Mann Whitney test at the 0.05 level of significance assuming homogeneity of variances of the two groups. For pair-wise comparisons of single-linkage distances, the Wilcoxon rank-sum test was used with Bonferroni's correction. It was found that the CORT group showed increased distances among the somatosensory, parietal, and frontal regions versus the VEH group, indicating looser coupling or decreased connectivity in those regions in the CORT group (corrected $p < 0.01$). Loosely connected visual cortices in the CORT group were also indicated in the single-linkage distance matrices (corrected $p < 0.01$). Additionally, it was observed that the left frontal and left/right somatosensory and parietal cortex were further apart functionally in the CORT group than in the VEH group, indicating reduced connectivity in the CORT group (corrected $p < 0.01$). We visualized the geometrical information about the altered brain network by computing a dendrogram (Fig. 2.7c-d). The dendrogram provides a visual representation of how and where the brain network changes. The colors of the lines in the dendrogram represent the distance to the 'giant' component (one final component in which all nodes are connected to each other) for each connected component. The dendrogram at the delta frequency revealed decreased coupling (at earlier filtration values, $\varepsilon = 0.6$-0.8) among the brain regions of the CORT group versus the VEH group. In the CORT group, a subnetwork consisting of somatosensory and parietal regions was formed at a higher filtration value (Fig. 2.7d), while the same subnetwork was established at an earlier filtration value in the VEH group (Fig. 2.7c). This result indicates that in the CORT group, more local clusters are present at earlier filtration values, while not forming a big network.

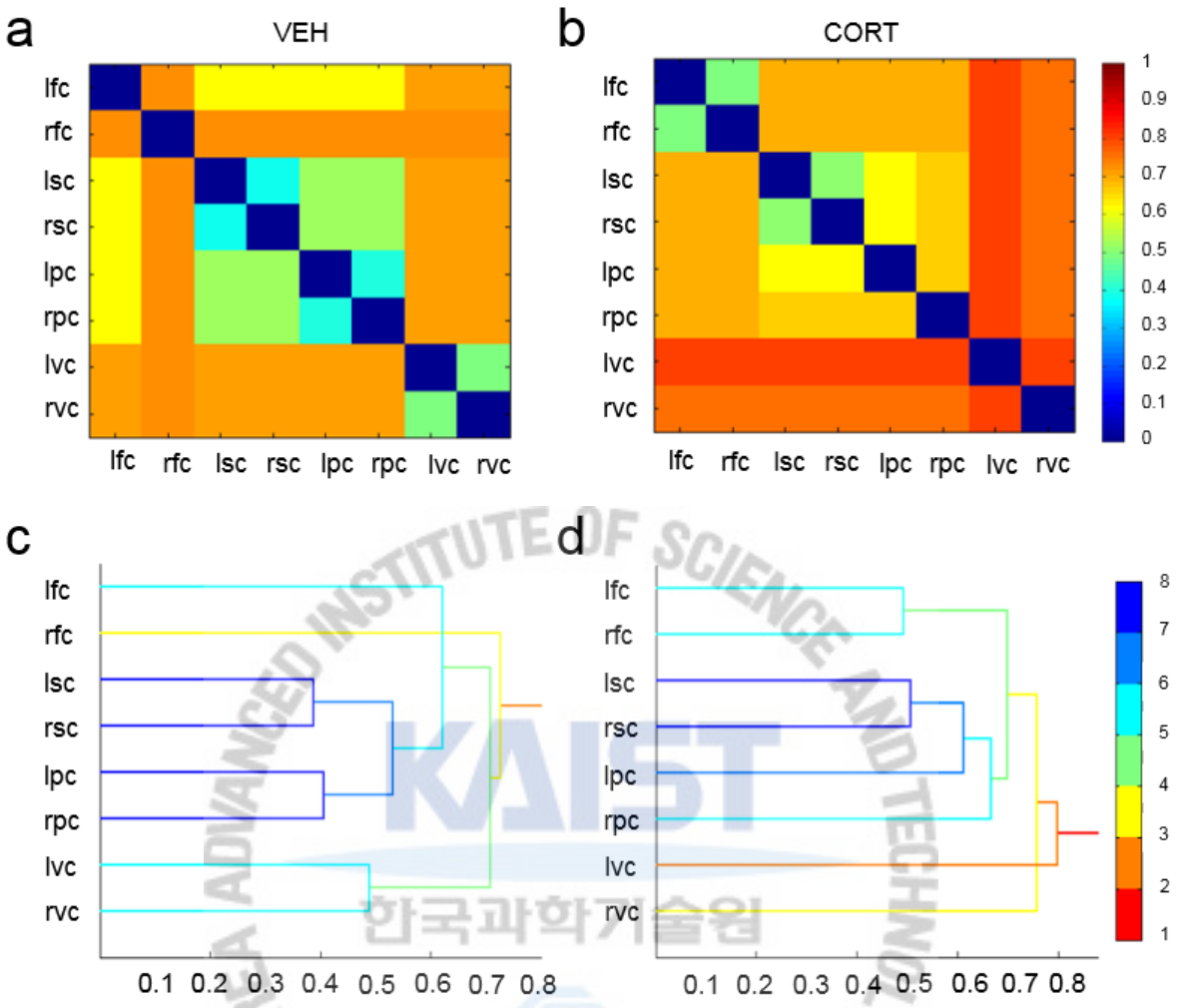

Figure 2.8: Increased functional distance and decreased functional connectivity is visualized by the single linkage matrices and dendrogram of the CORT group. (a, b) The single linkage matrices SLMs d_M for delta-frequency band of the VEH and CORT groups, with better illustration of group separation as compared to original distance matrices obtained from the Pearson correlation-based distance c_M in Fig.3 [43]. Intergroup comparison showing loose coupling between somatosensory and parietal cortices at 0.05 level of significance with two-tailed Mann Whitney test for exact probabilities. The single linkage dendrogram of the VEH and CORT groups is presented in (c, d). The vertical and horizontal axis represent node index and filtration value respectively. The color of lines shows the distance to the giant component. The distance to the giant component of the giant component is 1. Different subnetworks formation over the changing filtration values in both the groups can be seen. Hyperconnectivity of the frontal cortices while hypoconnectivity of visual

cortex in the CORT group can be seen from the dendrograms of both the groups. Also somatosensory cortices in the CORT group are making connections with other cortical circuitry at later filtration values yielding in decreased connectivity.

In Figure 2.8(a) model-predicted distance matrices (i.e., single-linkage matrices) for the theta-frequency EEG bands are shown. Decreased functional connectivity in the CORT group was seen among the various brain regions. Statistically significant pair-wise differences between the groups were shown using the Wilcoxon rank-sum test. In Figure 2.8(b) dendrograms for the theta-frequency EEG band are shown. In Figure 2.8(c), brain connectivity maps for the theta frequency are presented. From the geometrical information on connected nodes, the CORT group showed similar results to those of the delta-frequency band (i.e., more local clusters until higher filtration values). It can be seen that the connectivity map of the CORT group shows compromised coupling among brain regions at earlier threshold values (0.5, 0.6) and decreased connectivity strength at 0.8 compared with the VEH group. Cortical regions in the CORT group were making fewer connections in the evolution of the final network, as they became one large component at higher filtration values than in the VEH group. In the theta-frequency band, overlaying the barcodes along with the final filtration values (CORT group, 0.735; VEH group, 0.677) revealed significantly decreased global connectivity (0.05 level of significance, using the Wilcoxon rank-sum test on resampled data sets) in the CORT group (Fig. 2.8d). Furthermore, slope (CORT = 21.57) > slope (VEH = 18.16), which suggests that the CORT group had a more rapidly decreasing slope than the VEH group. Thus, the slope of the barcodes may not be useful when making inferences on the shape of barcodes.

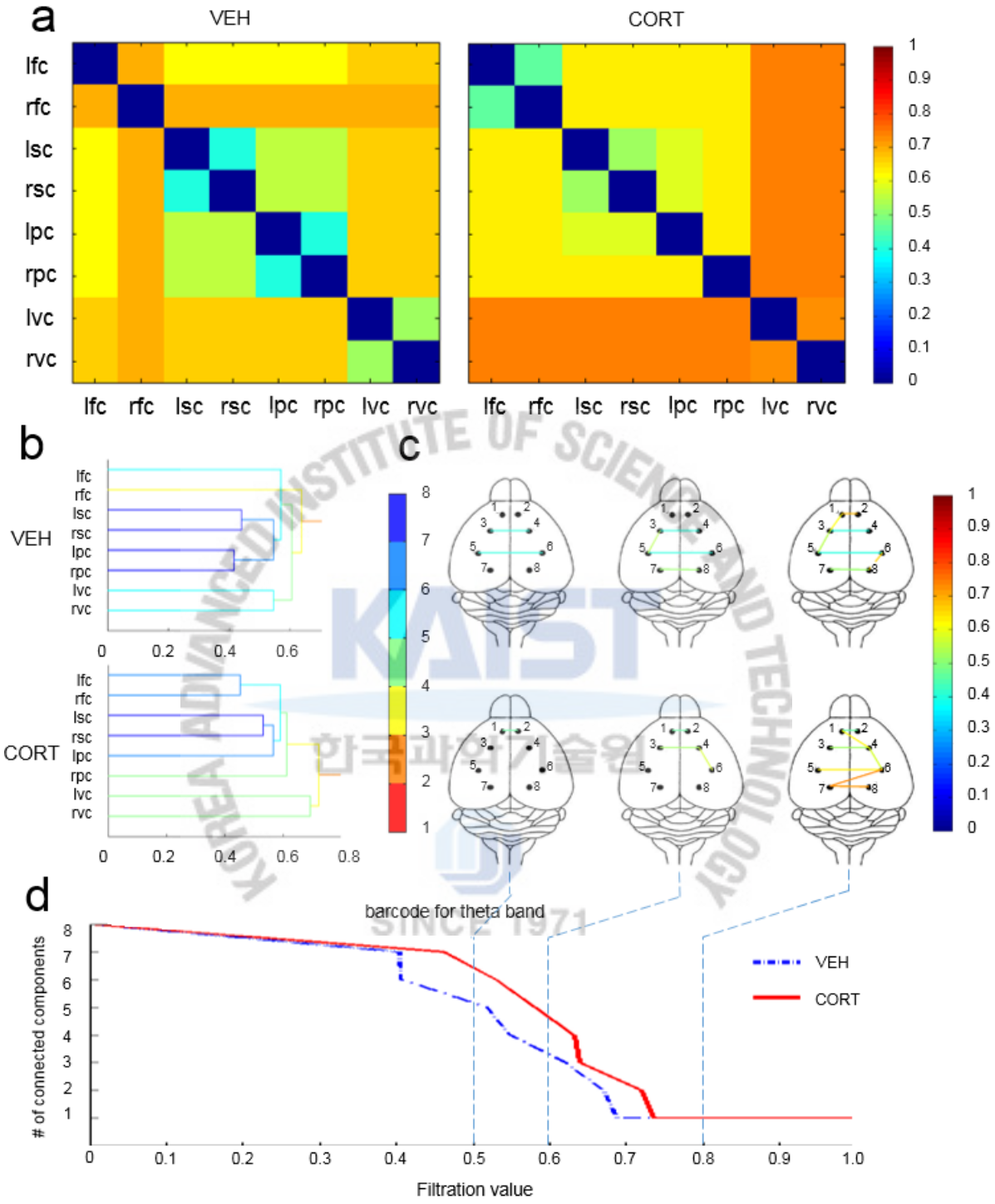

Figure 2.9: Trace of network evolution over changing filtration values at the theta-frequency band. (a) Single linkage matrices SLMs dM for theta frequency of the VEH and CORT groups. The loose coupling among different brain regions in the CORT group is presented and verified using Mann

Whitney test for exact probabilities. Single linkage dendrogram of the VEH and CORT groups is presented in (b). The vertical and horizontal axis represent node index and filtration values respectively. The color of lines shows the distance to the giant component. The distance to the giant component of the giant component is 1. (c) Connectivity maps of the VEH group and CORT groups at the filtration values ε=0.5, 0.6, 0.8 where color strength in the colorbar represents the functional distance between the nodes. Altered and decreased functional connectivity of the CORT group is shown in the brain network connectivity map. The overlaid barcodes of the VEH and CORT groups are tracing brain network evolution over the different filtration values in (d) where the final filtration value of the CORT group (= 0.7357) > the VEH group (= 0.6770) at 95% level of confidence with Wilcoxon rank-sum test of resampled datasets. Thus the CORT group depicts decreased global connectivity with 95% level of confidence.

The barcodes for the alpha-, beta-, and gamma-frequency bands and their slopes (CORT, 23.04 and VEH group, 25.49, CORT, 21.228 and VEH group, 33.29, and CORT, 21.47 and VEH group, 34.84, respectively) all showed that the VEH group had a steeper slope than the CORT group, yielding a faster decrease of the zeroth Betti number, or increased global connectivity in the VEH group. Furthermore, the final filtration values (alpha: CORT, 0.72 and VEH group, 0.63, beta: CORT, 0.6037 and VEH group, 0.7329, and gamma: CORT, 0.6847 and VEH group, 0.7489) revealed that the CORT group had a longer, heavy tail, indicating decreased global connectivity and more localized connectivity in the alpha, beta, and gamma frequency ranges (Fig. 7d, 8d, 9d). In Figures 2.9(a), 2.10(a), and 2.11(a), the model-predicted distance matrices (single-linkage matrices) for alpha-, beta-, and gamma-frequency EEG bands are shown, respectively.

Decreased functional connectivity in the CORT group was shown among almost all the distinct brain regions. The statistical significance of differences between groups was assessed using the Mann-Whitney test for exact probabilities with a Bonferroni correction. In Figures 2.9(b), 2.10(b), and 2.11(b), dendrograms for the alpha-, beta-, and gamma-frequency EEG bands are shown, respectively. Alpha-, beta-, and gamma-frequency-specific brain connectivity maps and other findings are also shown in Figures 2.9(c), 2.10(c), and 2.11(c), respectively. Similar connectivity profiles (decreased global and increased localized connectivity in the CORT group) but with different pathways among the cortical regions were seen in all five EEG frequency bands. Interestingly, the bilateral frontal cortices in the CORT group showed increased connectivity in the CORT group versus the VEH group at all five bands, which might indicate the spread of

depression severity because depression is characterized by increased functional connectivity within the frontal brain [44].

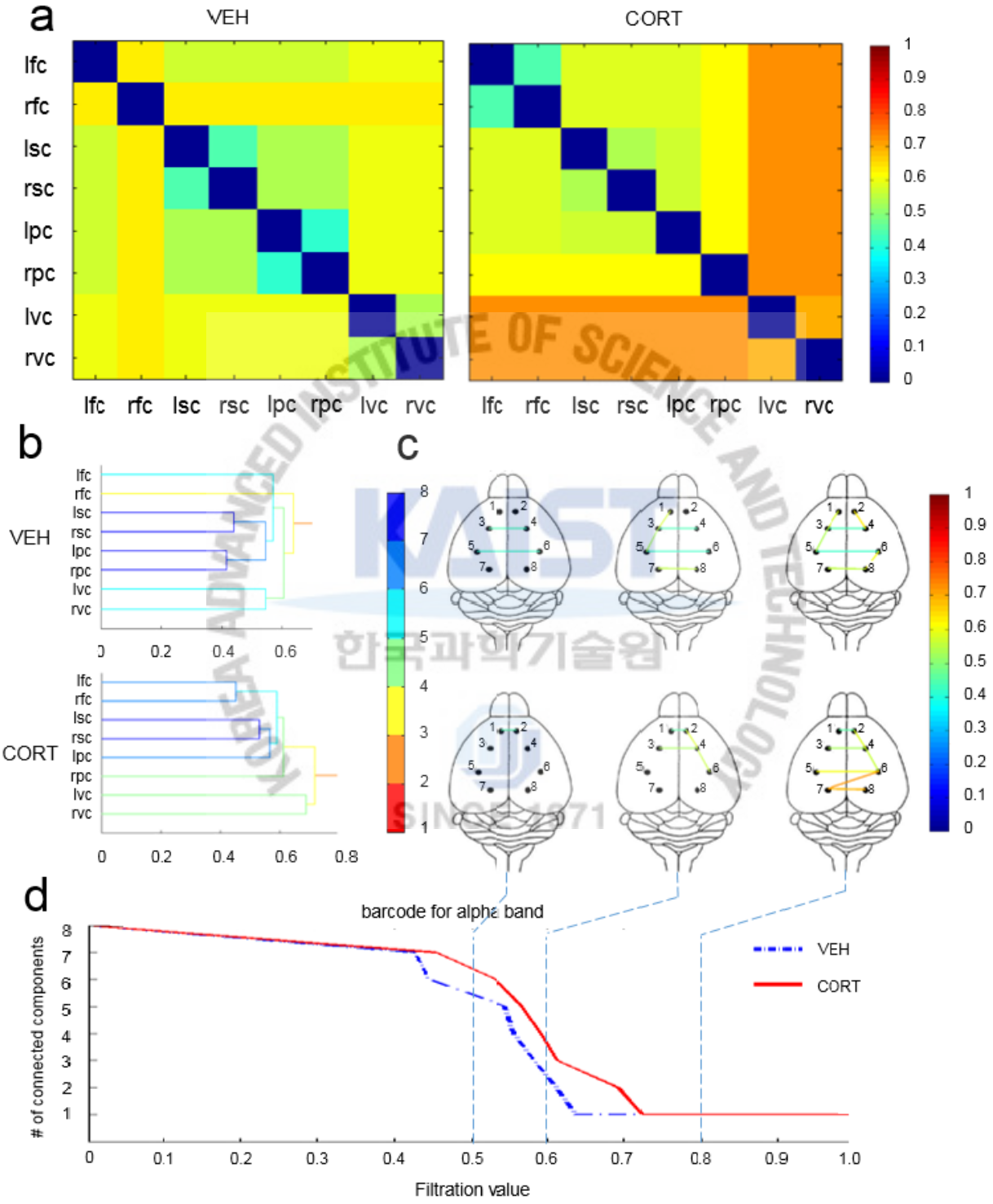

Figure 2.10: Trace of network evolution over changing filtration values at the alpha-frequency band. (a) The single linkage matrix SLM d_M of the VEH and CORT groups is presented in (a, b). Intergroup comparison was statistically done with 0.05 level of significance using Mann Whitney two tailed test for the exact probabilities. The single linkage dendrogram of the VEH and CORT groups is presented in (b). The vertical and horizontal axis represent node index and the filtration values respectively. The color of lines shows the distance to the giant component. The distance to the giant component of the giant component is 1.Altered connections in the CORT group as compared to the VEH group are depicted clearly by the dendrogram representation. (c) Connectivity maps of the VEH group and CORT groups at the filtration values ε=0.5, 0.6, 0.8 where color strength in the colorbar represent the functional distance between the nodes. Altered and decreased functional connectivity of the CORT group is depicted in the brain's connectivity map. Also, at alpha-frequency band the altered trend in somatosensory circuit with parietal and frontal cortex is evident from the connectivity map at filtration value 0.5 in both the groups. The overlaid barcodes of the VEH and CORT group are showing brain network evolution over the different filtration values in (d) where final filtration value of the CORT group (= 0.7224) > the VEH group (= 0.6362) at 95% level of confidence with Wilcoxon rank-sum test of resampled datasets. Thus the CORT group is exhibiting decreased global connectivity with 95% level of confidence.

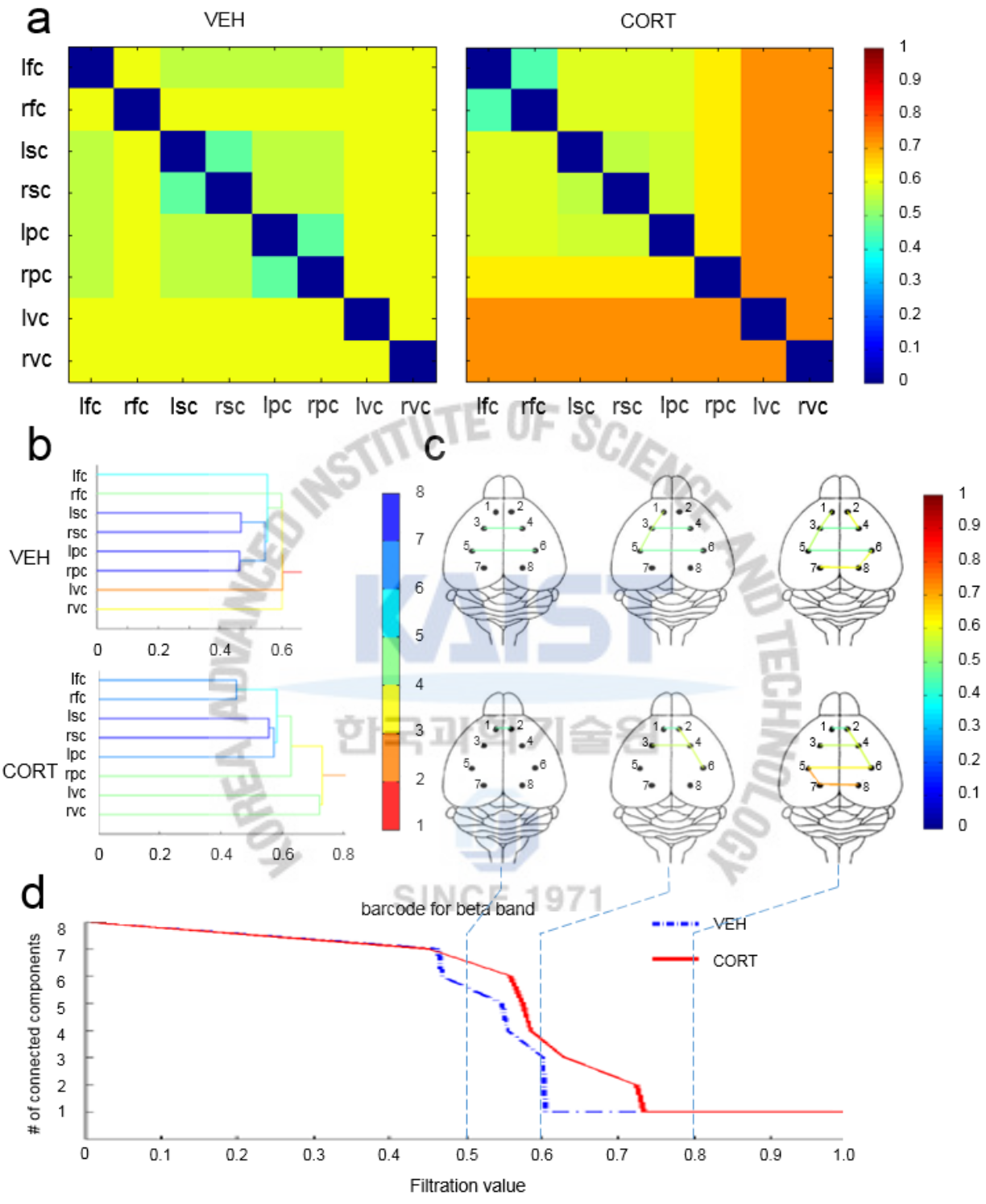

Figure 2.11: Network findings at beta frequency band. (a) Single linkage matrix for both the groups is presented, VEH (left) and CORT (right). (b) Single linkage dendrogram show altered connections among nodes of the CORT group (below) is shown when compared to the VEH group (upper). (c) Brain connectivity maps show over-local connectivity and decreased global connectivity for the CORT group. (d) Overlaid barcode of both the groups show significantly decreased global connectivity in the CORT group with a long tail since final filtration value for CORT (0.7329) > VEH (0.6037) at 95% level of confidence with Wilcoxon rank-sum test.

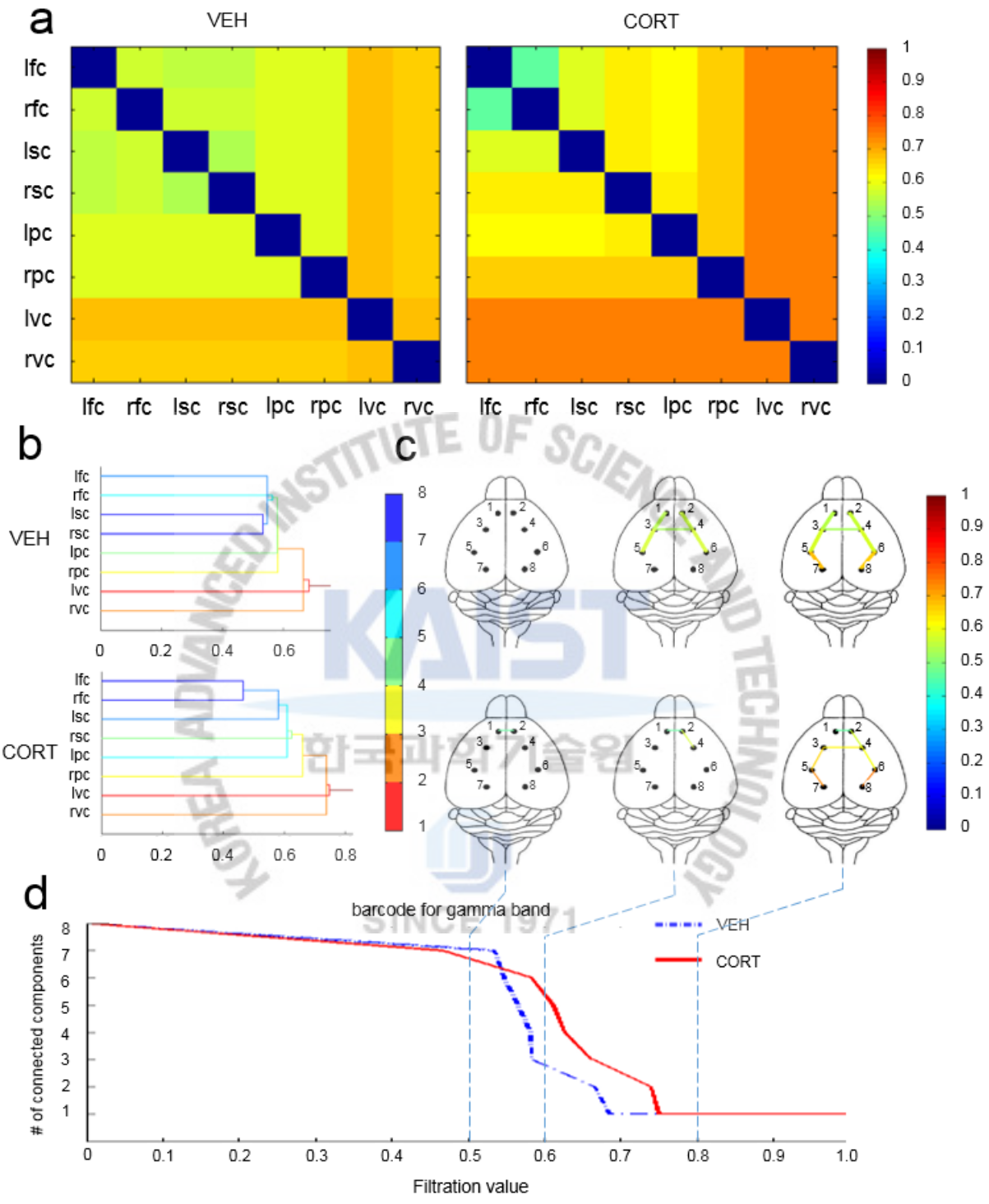

Figure 2.12: Network findings at gamma band. Similar connectivity profile as in other four frequency bands i.e., decreased global connectivity among cortical circuitry of the CORT group is shown. (a) Single linkage matrix for both the groups is presented, VEH (left) and CORT (right). (b) Single linkage dendrogram show altered connections among nodes of the CORT group (below) is shown when compared to the VEH group (upper). (c) Brain connectivity maps show over-local connectivity and decreased global connectivity for the CORT group. Whereas, hyperconnectivity of frontal cortices at earlier filtration value (=0.5) is evident. (d) Overlaid barcode of both the groups show significantly decreased global connectivity in the CORT group with a long tail since final filtration value for CORT (0.7489) > VEH (0.6847) at 95% level of confidence with Wilcoxon rank-sum test.

2.5.1 Comparison with other graph theoretic measures

Gromov-Hausdorrf (GH) distance:

After constructing the brain network we need to compute the distance between the networks for quantification. To compute the GH distance, we need to determine the correspondence between two different metric spaces (X,d_x) and (Y,d_y) [32, 45]. In our brain network model, the node sets X and Y is given in the fixed identical locations in the template. Therefore, the node $x_i \in X$ is simply mapped to $y_i \in Y$. Therefore, GH-distance can be trivially characterized as

$$d_{GH}(X,Y) = \frac{1}{2}\max_{\forall i,j} \left| d_X(x_i, x_j) - d_Y(y_i, y_j) \right|.$$

The GH_distance is the maximum difference between two SLMs when the order of column and row vector is fixed.

To validate the approach of persistent brain network homology with other available graph theoretic approaches, we constructed 10 and 9 networks for the VEH and CORT groups, respectively. For all (10 + 9) networks, we obtained seven distance matrices between the networks, including the Gromov-Hausdorff distance, between all pair wise single-linkage matrices along with pair wise differences between six other graph theoretic measures: the slope of barcode β_0, the characteristic path length, the average assortativity, the average clustering coefficient, the modularity, and average node betweenness centrality Figure. 2.13. All distance matrices were normalized to have a maximum value = 1. After constructing the distance matrices, we divided the networks into two

clusters and evaluated the clustering accuracy by comparing the assigned labels with the true labels. The clustering accuracies of the GH distance and the characteristic path length were both 100%, superior to the other widely used graph theoretic measures, indicating effective performance of the GH metric Figure. 2.13.

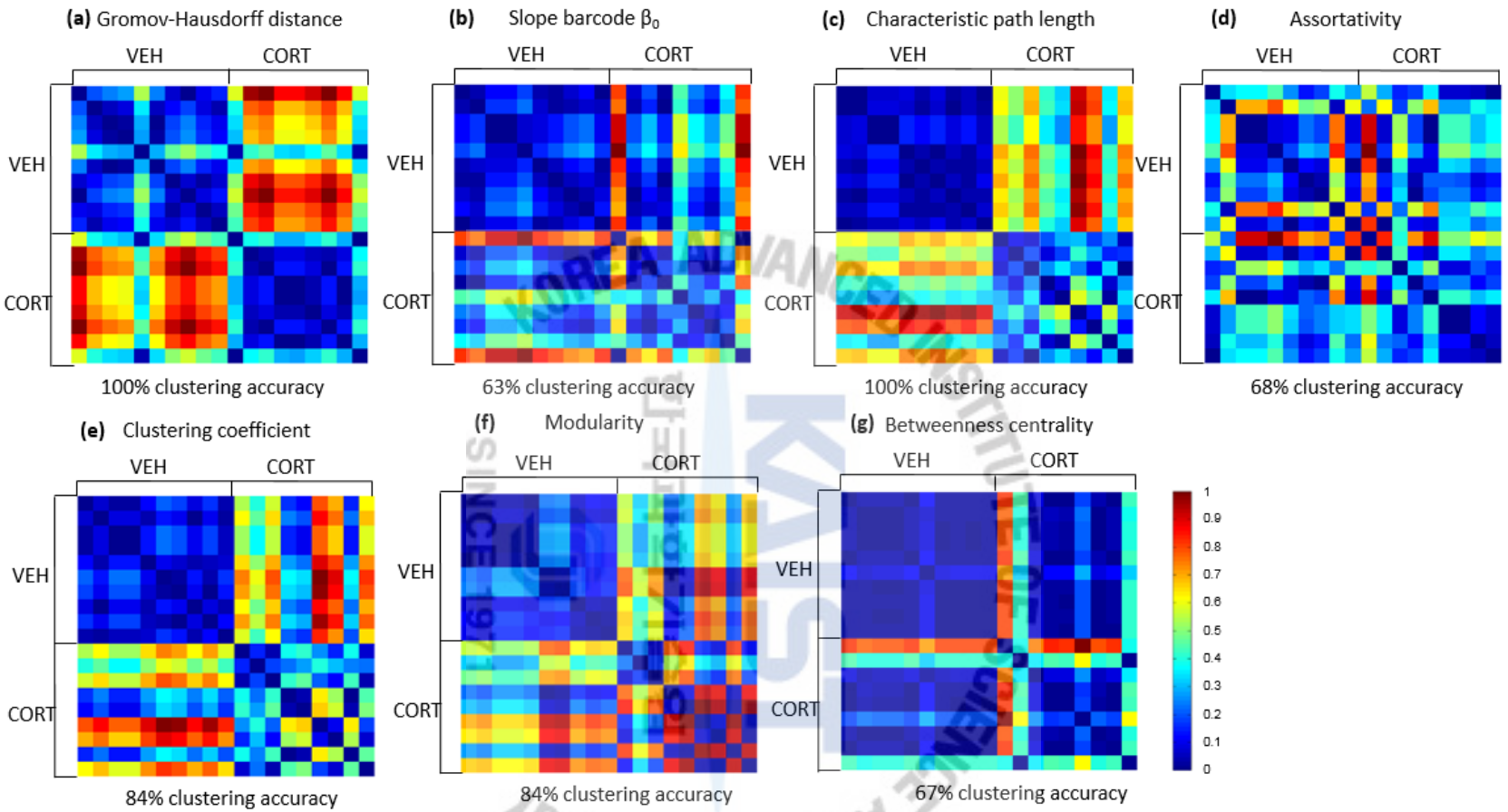

Figure 2.13: Comparison of 7 different methods: (a) GH distance, (b) Slope of barcode β0 (c) Characteristic path length (d) assortativity (e) clustering coefficient (f) modularity (g) betweenness centrality. In each distance matrix diagonal block refers to the distance between networks within a group and off-diagonal matrices measures the distance between different groups. From (a) to (g) the clustering accuracies are 100%, 63%, 100%, 68%, 84%, 84% and 67%. The GH-distance shows high efficiency.

2.6 Discussion

To assess brain functional connectivity, persistent brain network homology, a new multi-scale network-modeling framework [32], was used effectively with EEG signals from the CORT-induced depression mouse model. Persistent brain network homology uses networks generated at every possible threshold, and thus eliminates the need for an optimal threshold, which is a key factor in constructing binary networks. Furthermore, the persistent homology approach can allow geometric information in the barcode to be incorporated into a single-linkage dendrogram that represents the brain network changes visually. Thus, 'hidden' or abnormal neural networks in the pathological brain can be revealed by the persistent brain network homology approach.

In this study, application of persistent homology in eight cortical regions revealed more localized and decreased global connectivity in the CORT group versus the VEH group. Additionally, connectivity maps with single-linkage distances showed reduced and highly discriminated functional connectivity in the subregions in the CORT group. Our study demonstrated less integrated processing of effective information in cortical brain regions of the CORT group, and our results may facilitate investigation of the mechanisms underlying aberrant neural networks in the depressed brain.

Functional connectivity in the brain can be measured by statistical dependencies among the physiological signals from the coupled neural systems. In the healthy brain, individual variability in cognitive functions, learning a new task, and even the predisposition to learn have been correlated with specific patterns of connectivity within/across networks. In the diseased brain, specific abnormalities in neural networks even in structurally normal regions, may correlate with functional deficits, and functional connectivity has been used to assess impairment in neural communications [25, 46, 47].Depression may be associated with disturbed properties across large-scale cortical networks and/or subcortical systems with a number of functionally connected cortical regions [48, 49].Measurement of electrical activity, such as by EEG, has been used for research into brain functional connectivity, and many studies have suggested that alterations in EEG functional connectivity of patients with brain disorders, including depression, may be associated with cognitive dysfunction and psychiatric behaviors [10, 50]. However, tracing global

networks through the evolution of local subnetworks, where selection of the optimal threshold can be a problem, is difficult.

The persistent homology analysis, with the help of barcodes at all five EEG frequency bands, showed more localized and decreased global connectivity in the CORT mouse model. Additionally, the geometrical information-based dendrogram showed altered and compromised functional pathways in the somatosensory, frontal, and parietal cortices during formation of a large network. In fact, there is a report that patients with depression have limited affective processing and fewer redundant, or simply a reduced number of, connections among those cortical regions [51]. At each frequency band, a single-linkage distance matrix showed decreased connectivity among the left frontal and parietal cortices of the CORT group. Because the parietal lobes are themselves closely interconnected with the prefrontal areas, and, together, these two regions represent the highest level of integration in the motor control hierarchy, decreased connectivity in these regions may lead to impairment in cognitive function, including decision-making. Moreover, bilaterally looser connection at the visual cortex and increased connections in the frontal cortex in the CORT group were also seen with single-linkage distance matrices. Although the CORT group showed a similar trend in local and global connectivity (i.e., more localized and less global connectivity) in all frequency bands versus the VEH group, there were some differences in the connectivity pathways between the groups.

The dynamics of coupled oscillatory systems from each frequency band are useful for maintaining different functional sub-networks in a state of heightened competition, which can be stabilized and changed by even slight modulation of sensory or internal signals [52, 53]. The underlying temporally correlated patterns of frequency-specific brain oscillations or activities are still not understood fully, and thus their purposes remain unclear at this time. As future investigations delve deeper into the origins and possible functions of frequency-related brain EEG activities, we will be able to comprehensively investigate brain function within frequency-specific brain networks.

To date, various animal models (e.g., CORT treatment, chronic restraint stress, inescapable foot-shock stress, chronic social defeat stress, chronic unpredictable mild stress) have been established to facilitate understanding of the pathophysiology of depression [54]. Although not without limitations, certain depression-associated phenotypes can be reproduced independently and

evaluated in a mouse model. The CORT-induced depression mouse model used in this study is known to reproduce human behaviors, such as despair, anhedonia, or helplessness, which are regarded as face validity and which can be reversed by antidepressant treatment [38, 39]. However, depression is a heterogeneous disorder of which the diagnostic criteria are partially subjective. Thus, we cannot generalize our findings to specific clinical impacts in depression patients. To enable translation of the results, further research on the persistent brain network homology of clinical depression is essential.

2.7 Conclusion

In this study, we investigated cortical functional networks from multiple cortical EEG signals of the CORT-induced depression mouse model, and demonstrated substantially altered functional connectivity in the CORT model. Use of the persistent brain network homology approach that considered all networks over every possible threshold enabled identification and quantification of increased local and decreased global connectivity of complex brain networks in the CORT model. Furthermore, loose coupling of somatosensory and other cortical regions and compromised functional connectivity between visual and other cortical regions were also revealed, which might contribute to deficient filtering or processing of information within brain regions in depression. Our study suggests the utility of the persistent brain network homology approach for tracing the evolution of EEG functional connectivity in neuropathological brain mapping, as well as the compromised functional connectivity in the CORT-induced depression model.

Chapter 3 . Gamma oscillation in functional brain network is involved in spontaneous remission of depressive behavior

3.1 Introduction

Depression is common mental disorder that affects approximately 121 million people worldwide and is considered one of the leading causes of disability (WHO 2008). Individuals suffering from depression have increased physical illness, decreased social functioning, and a high mortality rate, resulting in huge social and economic strain (reviewed in [55]). Although numerous ways of treatment such as pharmacotherapy, cognitive behavioral therapy and psychotherapy have been developed, up to one third of patients are non-responders to most currently used methods [56, 57]. This response rate underscores the importance of developing neurophysiologic predictors of remission in depression, which would ultimately increase the potential for personalized medical treatment for these patients (reviewed in [58]. Further, the pursuit of predictors for treatment response in depression research has been going on for decades, yet with only modest success. Both, prescriptive (i.e. predicting differential response to one versus another treatment) and prognostic (i.e. predicting response to a particular treatment) predictors from various domains were identified in the literature [43]. However, when looking at the comprehensive meta-reviews [59-61], most results of the original studies are conflicting and this is now a major obstacle in the quest to modernize diagnosis and treatment in this field.

No consensus has been reached on the exploration of network-level functional connectivity as a predictor of spontaneous recovery in depression. Thus the effects of spontaneous recovery from depression upon functional connectivity in the delta through gamma spectra, the frequency domains most typically held to underlie neuropsychological functioning, appear not to have been studied much. First, when exist, spontaneous recovery would be likely to affect brain functions that are typically altered in severe depression. Second, the involved mechanism should be affected for a time period that matches the average endurance of clinical effects, which is indicated to be several days to a few weeks. In considering this evidence, we hypothesize that spontaneous recovery may alter the functioning of temporal oscillations on a network level which may predict the recovery of affected brain. To identify effects upon cortical regions' functioning we

investigated and analyze EEG of the depression mouse model recorded after three weeks. In this study, chronic restraint stress (CRS) was used to induce a mouse model of depression. The physical stress caused by chronic restraint is known to induce depression-like behaviors in rodents. In addition, previous study reported that CRS-induced mouse model of depression shows spontaneous recovery of depression-like behaviors to normal level [62] which provides a simple method to perform the intragroup comparison of depressed state with depression-recovery state. We found that CRS-induced behavioral deficits were spontaneously recovered during a post-CRS period, which is consistent with the previous report [62]. Forced swimming test (FST) for despair-like behavior and open-field test for locomotor activity and anxiety were conducted at 1 week (CRS1W group) and 3 weeks (CRS3W group) following the cessation of 4-week-CRS (**Fig. 1a**).
For tracing the evolution of the altered and recovered functional network in depressive brain, persistent homology can serve as the powerful analysis tool. Further, along with the network-level functional connectivity, effective (causal) connectivity is explored to observe directed causal interaction between the two brain regions and to mark the most influential network of brain's region in spontaneous recovery.
We have found that in the CRS3W group traversed functional connectivity between somatosensory and frontal cortices at the gamma frequency range may be a potential predictor of remission in the depressive mouse model.

3.2 Material and methods

3.2.1 Animals

Adult male C57BL/6 mice (7-8 weeks old) were used for the generation of chronic restraint stress (CRS)-induced mouse model of depression. All mice were housed under a 12-h light/dark cycle and had ad libitum access to food and water. Animal care and handling were carried out according to the guidelines approved by the Institutional Animal Care and Use Committee at the Korea Advanced Institute of Science and Technology (KAIST).

3.2.2 Generation of CRS-induced depression mouse model and behavioral task

CRS procedure was designed and conducted in line with a previous study [62]. Timeline of CRS is illustrated in Fig. 1a. For the restraint of mice, each mouse was placed in a 50 mL polystyrene tube that has evenly spaced 9 vent-holes (0.5 cm diameter each; 1.0 cm apart from each other) for 6 h, and then the restrained mice were placed in their home cage. Mice experienced restraint once a day from Day 1 to 28 (4 weeks). After 1 (CRS1W) or 3 weeks (CRS3W) (a post-CRS period) following the cessation of the 4-week-CRS, mice were subjected to behavioral tasks. Forced swimming test (FST) was used to measure behavioral despair, an indicator of depression-like behavior in mice [39, 63]. Briefly, mice were placed individually in 2000 ml glass beakers filled with nearly 1400 ml of water (10 cm from the ground, with water temperature of 25 ± 1 °C) and were allowed to swim freely for 6 min. The duration of immobility was measured during the last 4 min of the task. All behavioral tests were video-recorded. For the measurement of locomotor activity (total distance moved) and anxiety level (time in center), open-field test was performed as described previously [41, 64].Briefly, mice were put in an open-field box made of white plastic walls (40cm × 40cm × 40cm) and each mouse was placed in the periphery of the field. Then during the 10-min of video-recorded session, the total distance traveled and the time spent in the center of the box were analyzed with EthoVision (Noldus Information Technology, Wageningen, Netherlands).

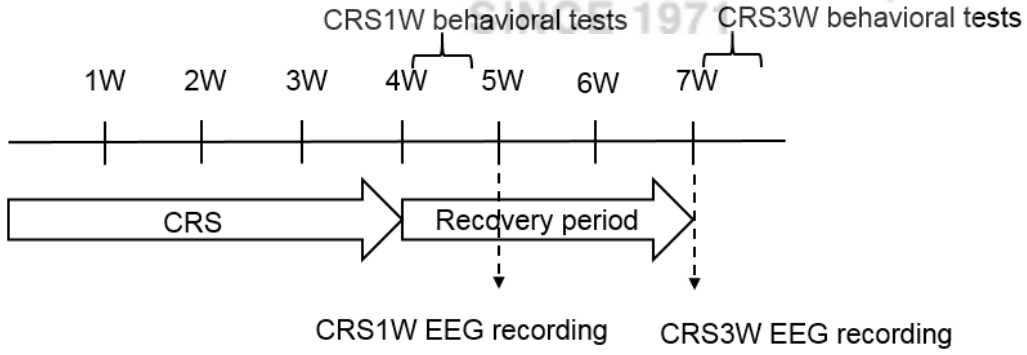

Figure 3.1: Schematic for behavioral tasks and EEG recordings.

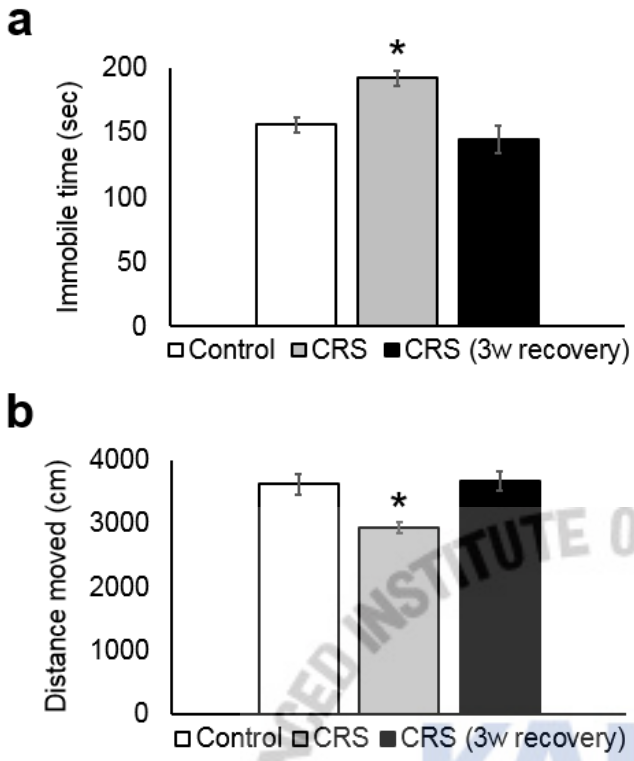

Figure 3.2: Depression-like behaviors in mice subjected to CRS, and spontaneous recovery of depression-like behaviors after recovery from CRS. (**a**) CRS group (n=9) showed increased time spent immobile in FST compared to both control (n=10) and CRS-recovery groups. *P<0.01 by Student's t-test. CRS-recovery group (n=11) showed complete recovery of depression-like behavior in FST when compared to the control group. (**b**) Decreased locomotor activity was observed in CRS group (n=9) compared to control (n=10) and CRS-recovery groups in the open-field test. *P<0.01 by Student's t-test. Again, there was no significant difference between control and CRS-recovery groups, indicating the recovery of locomotor activity.

3.2.3 Functional connectivity analysis

Continuous EEG signals from the animals, each consisting of 1 min of data from last day of recording, in which they were in a resting state (i.e., awake and no movement), were analyzed. The five EEG frequency-bands—delta (1.5-4Hz), theta (4-8Hz), alpha (8-12Hz), beta (12-30Hz), and gamma (30-80Hz)—were analyzed for power density and functional connectivity.

Cross-correlation: For cross-correlation analysis, the measurement set is denoted as M = $\{m_1, m_2, \ldots, m_8\}$ consisting of eight nodes (i.e., eight brain regions) where we have measurement m_i at the i^{th} node. We calculated cross-correlation matrix through the following equation:

$$corr(m_i, m_j) = \left\langle \frac{m_i}{\|m_i\|}, \frac{m_j}{\|m_j\|} \right\rangle$$

Persistent brain network homology: We used multiscale network modelling technique known as persistent brain network homology to compare the networks of CRS models and controls effectively. Detailed procedures to quantify topological features based on persistent homology were described in a previous study [32, 64]. In brief, we used networks generated at every possible threshold and to seek evolutionary changes in the subnetwork clusters by increasing the threshold in correlation matrix, which was visualized by dendrogram. The distance matrix c_M between two EEG measurements m_i and m_j through the following equation:

$$c_M(m_i, m_j) = \sqrt{1 - corr(m_i, m_j)}.$$

The brain network can be viewed as the weighted graph (M, c_M) where M is a set of measurements at each brain region (= node) and c_M is the metric defined on that set. We connect the nodes i and j with an edge if the distance c_M (mi, mj) ≤ ε for some threshold value ε. Then the binary network B(M,ε) at threshold ε is a graph consisting of 0-simplices (nodes) and 1-simplices (edges). Start with ε = 0 and increase the ε at each iteration. The value of ε is taken discretely from the smallest $c_M(m_i,m_j)$ to largest $c_M(m_i,m_j)$. By increasing ε, more connected edges may be involved. If two nodes are already connected directly or indirectly via other intermediate nodes in smaller ε then at larger ε we don't connect them. As a topological view of brain network, Rips complex was used to represent simplical complexes. Rips complex is defined as a simplical complex consisting of nodes and edges, whose k-simplices correspond to edges as a (k+1)-simplices which are links of two nodes within the distance ε. Rips filtration reflects the multiscale networks, the sequence of nested Rips complexes over different scales. One of the topological features, Betti number β_0, is a measure of the number of the connected components in the network. We could visualize those topological changes using barcode and dendrogram according to β_0. We consider the network consisting of 0− and 1−complexes (nodes and edges). Our main concern is the changes of the zeroth Betti number β_0, which measures the number of connected networks (CNs). The changes

of β_0 are visualized using the barcode. The vertical and horizontal axes in the barcode represent the indices of CN and filtration values respectively. The barcode of β_0 is basically a decreasing function showing when CNs are merging to form a bigger network component. The number of CNs at the certain filtration value is same to the number of bars. If we rearrange the bars according to the node index instead of CN index in the vertical axis, we obtain single linkage dendrogram (SLD). While the barcode of β_0 shows the global changes of the connected structure of network when the bars are ended, the SLD shows the local changes when the bars are merged. SLD between the nodes was calculated, which is usually used in hierarchical clustering. Given the network with distance c_M, we calculated SLD (d_M), which was defines as:

$$d_M(m_i, m_j) = \min\{\max_{l=0,\cdots,k-1} c_M(w_l, w_{l+1}) / m_i = w_0, \cdots, w_k = m_j\}$$

where mi = w0,…,wk = mj be a path between mi and mj. SLD is the minimum distance between two nodes when they belong to the same connected component during Rips filtration. It represents the hierarchical clustered structure of brain network in an algebraic form which can be used for a quantitative measure to discriminate brain networks. Using SLD calculated from persistent network homology, we could obtain the distance between two nodes after network construction without specific threshold.

3.3 Results and Discussion

3.3.1 EEG Power

The power density spectra were calculated using fast Fourier transform (FFT) analysis. The normalized power (for intergroup comparison) of 5 frequency bands (delta: 1.5~3.9, theta: 4~8, alpha: 9~12, beta: 13~30, low-gamma: 31~80Hz) was analyzed. Electrode wise power analysis showed statistically significant (*: $p<0.05$) differences between the ctrl (control group) and the CRS1W group (corticosterone-induced depression model group) in the right somatosensory cortex at all frequency ranges other than the theta and alpha band (figure 3.3). This statistical difference disappeared in CRS3W group, as depicted by EEG power for CRS3W is not significantly different from the ctrl group (Fig.3.3). Other cortical regions included in this study did not show any statistical different powers in CRS1W and CRS3W. Although there were few significant power

changes in the ctrl and the CRS1W group which disappeared after three weeks but those recovered powers were not different with CRS1W when compared statistically.

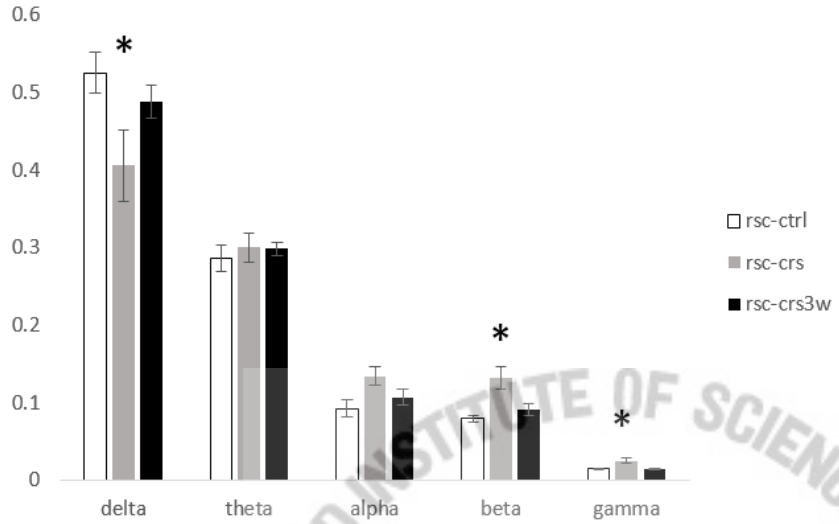

Figure 3.3: Normalized power bar chart for all three groups. The CRS3W group is showing traversed power indicating restored power spectrum of recovered group when compared to the control group. Here * indicates 0.05 level of confidence tested with ANOVA.

3.3.2 Functional Connectivity

Cross correlation was calculated between all pairwise nodes to quantify the functional connectivity. Pearson's correlation coefficient was used to obtain correlation values at zero lag. First peak analysis in cross correlation showed several statistically increased correlations between nodes at all five frequency bands in the control and the CRS1W group (Fig.3.4 b top rows). In general, CRS1W group showed increased connectivity as compared to the control group ($p<0.05$). After three weeks the delta, and gamma frequency ranges depicted traversed correlations when compared between the control and the CRS3W group (Fig.3.4 b last row). All statistical differences in correlation are disappeared. Our hypothesis is to access recovery of functional connectivity mainly in somatosensory cortices at gamma frequency band, when examined somatosensory nodes in the gamma connectivity matrices we found somatosensory at gamma frequency as probable predictor of spontaneous recovery in depression ($p<0.05$, Kruskal wallis). Whereas, theta-, alpha-,

and beta-frequency ranges could not show recovered connectivity but more differences appeared between the control and CRS3W group ($p<0.05$, Kruskal wallis) (figure 3.4).

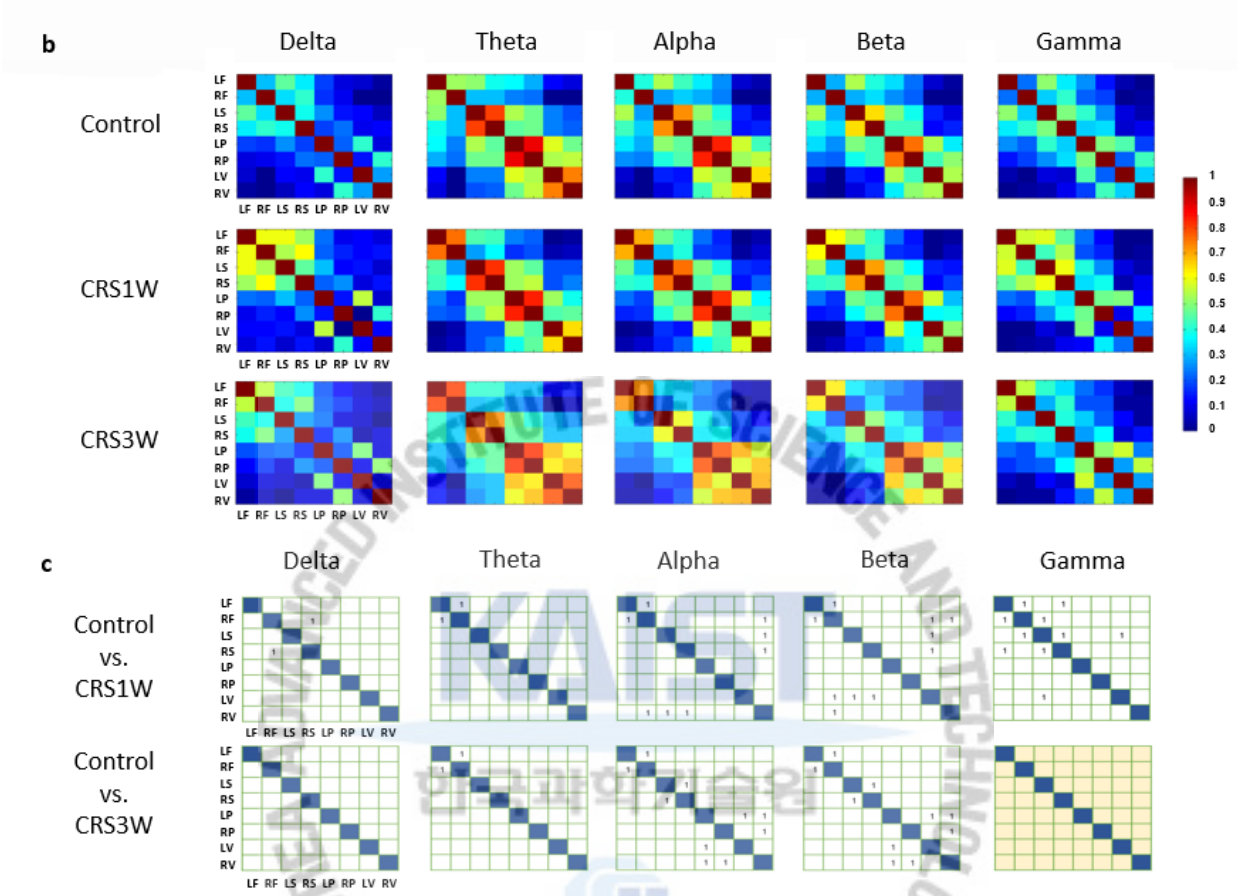

Figure 3.4: Cross correlation analysis showing remission at gamma frequency range in the CRS3W group. (a) Connectivity matrices between all pairwise nodes, where color strength is directly referring to the connectivity strength. In several regions of the brain, connectivity profile is restored in the CRS3W group at delta- and gamma-frequency ranges. (b) Pictorial representations for statistical values between control and CRS1W (above row), control and CRS3W (below row). Where there is significant difference (tested with Kruskal wallis multiple comparison) among groups, the cell is filled with '1'. The comparison of control and CRS3W is showing that all the differences at delta and specifically gamma band, are all vanished after 3 weeks.

3.3.3 Network Analysis

Then, we used a multiscale network approach, persistent brain network homology, to investigate brain connectivity at the network levels before and after spontaneous remission of depressive-like behaviors. The single-linkage matrix showing the predicted distance among 8 brain regions could produce efficient separation of the brain subnetworks within each group Figure 3.5. The CRS1W group had decreased functional distance between many regions at different frequency bands compared with the control group, indicating an increased functional connectivity in the CRS1W group Figure 3.5.

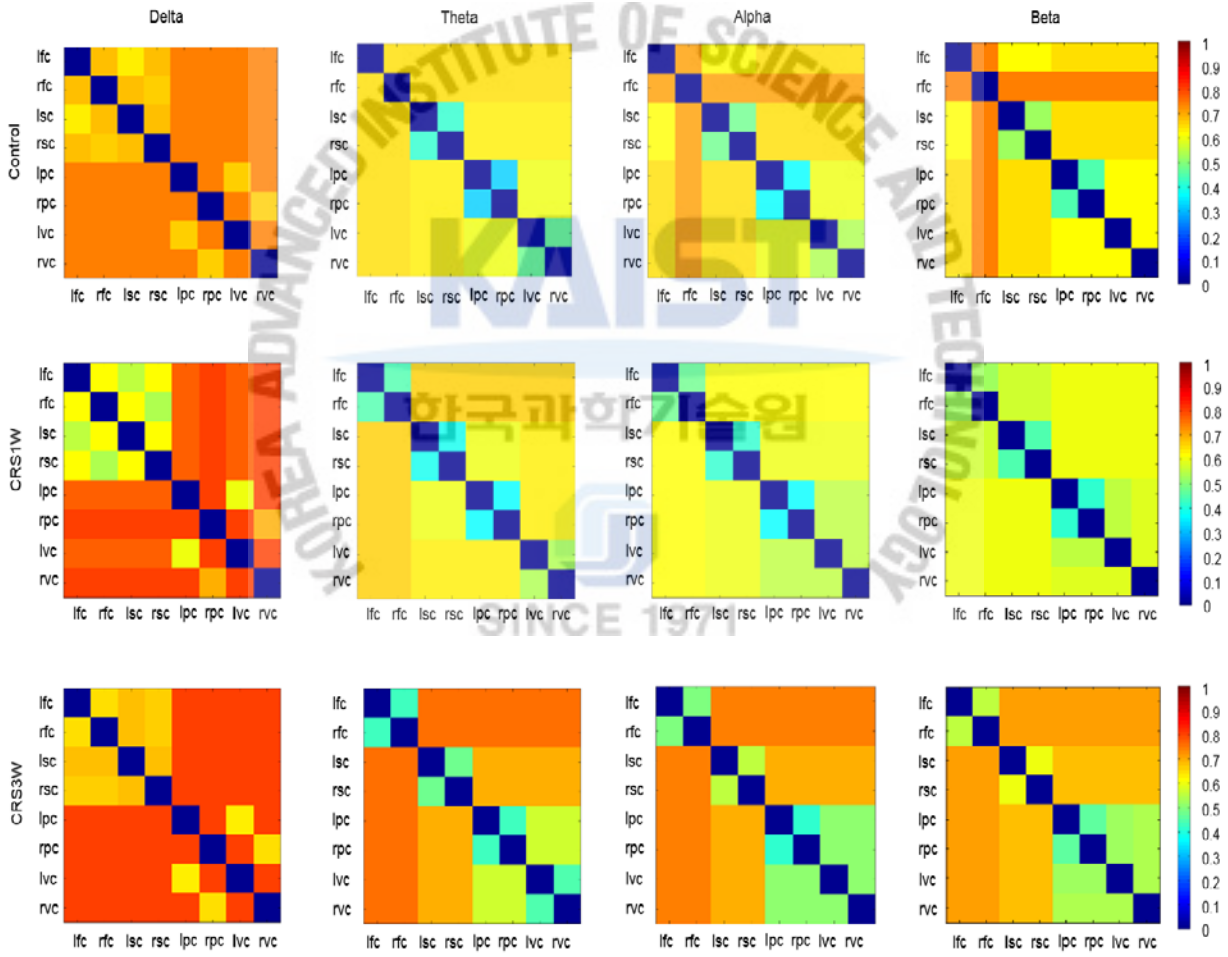

Figure 3.5: Single Linkage matrices at delta-, theta-, alpha-, and beta-frequency bands for all three groups. No recovery in any of these ranges were recorded, but more differences appear between the Control and CRS3W group (95% level of confidence using Kruskal Wallis test).

Interestingly, however, the CRS3W group displayed a restoration of the decreased distances only at gamma-frequency band (**Fig. 3.6a**). The CRS1W group showed decreased functional distances (i.e., increased connectivity) mainly among the somatosensory and frontal cortices, but the CRS3W group showed similar functional distances in those regions with the control group (**Fig. 3.6a**). The decreased functional distances among the parietal and visual cortices in the CRS1W group were also depicted in the single-linkage distance matrices, which was not recovered in the CRS3W group. We further examined brain networks at gamma-frequency band by depicting barcode for evolution of networks and dendrogram for single-linkage hierarchical clustering, respectively. We also drew brain maps containing the functional connectivity. In the overlaid barcode, the control (= 0.697) and CRS3W (= 0.700) groups showed a similar final filtration value (i.e., maximum single-linkage distance), but the CRS1W group (= 0.682) exhibited a lower final filtration value compared to other groups (**Fig. 3.6b**), indicating increased global connectivity in the CRS1W group. By constructing a dendrogram (**Fig. 3.6c**) and connectivity map (**Fig. 3.6d**), we could provide a visual representation of where and what brain subnetworks change or recover. Interestingly, the subnetworks consisting of the somatosensory and frontal cortices were formed at the earlier filtration values (between $\varepsilon = 0.50$ and $\varepsilon = 0.55$) in the CRS1W group (**Fig. 3.6c**), which was also displayed in the brain connectivity map at the filtration value $\varepsilon = 0.55$ (**Fig. 3.6d**). However, the control and CRS3W groups did not show any subnetwork couplings at the same filtration-value ranges (**Fig. 3.6c,d**). In addition, at the filtration value $\varepsilon = 0.75$, in which all groups showed all connections among 8 cortical regions, the CRS1W group exhibited increased strength of functional connectivity in the somatosensory and frontal cortices. However, the CRS3W group depicted similar strength of connectivity among those cortices compared with the control group (**Fig. 3.6d**), representing the recovery of the strength of functional connectivity in the CRS3W group.

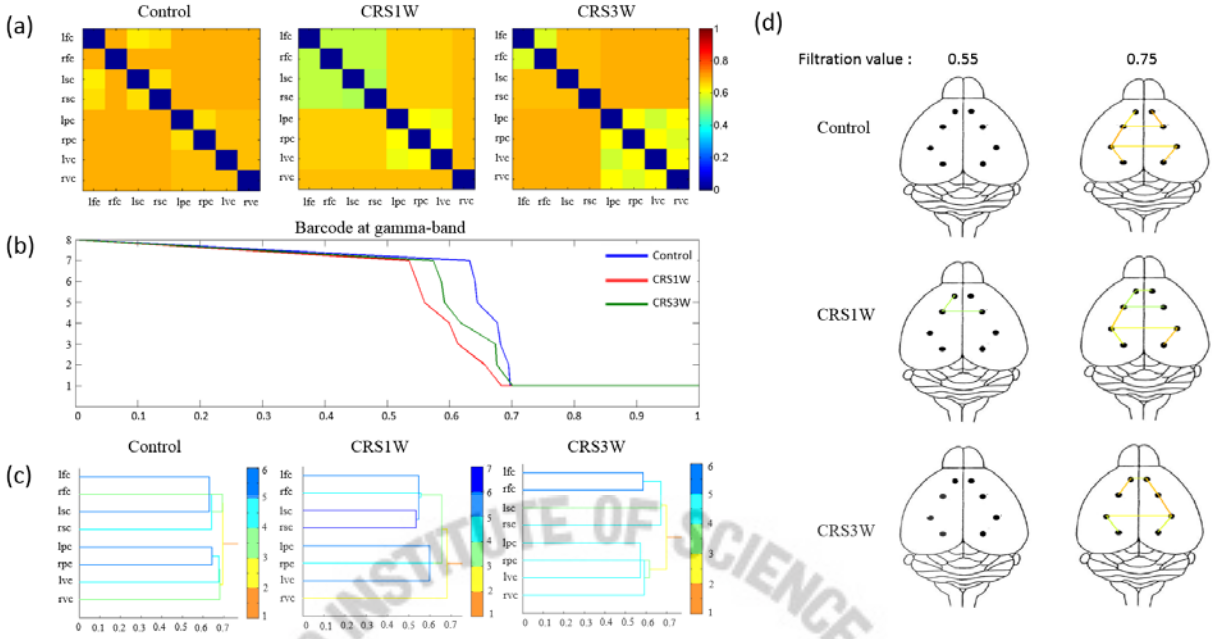

Figure 3.6: Network findings at gamma band using persistent brain network homology. (**a**) Single linkage matrices are shown to have increased functional connectivity in the CRS1W group particularly between somatosensory and frontal cortices ($p<0.01$, Kruskal wallis test) which is significantly decreased in CRS3W as compared to the CRS1W ($p<0.01$, Kruskal wallis test) and having no difference when compared CRS3W and the control group. (**b**) Overlaid barcodes for the control, CRS1W and CRS3W are presented. The CRS1W group exhibiting increased global connectivity as all components to merge in one big network at earlier filtration value (=0.6827) than the control group (final filtration value=0.6971). The network evolution for CRS3W is seen to traverse to the control group suggesting probable recovery. (**c**) The dendrogram marking the traversed connectivity pathways between control and CRS3W groups. (**d**) Brain connectivity maps for control, CRS1W and CRS3w at filtration value 0.55, and 0.75. The CRS1W group showed decreased functional distance (increased functional connectivity) as compared to the control group, which was restored particularly between somatosensory and frontal cortices after three weeks as shown in the connectivity maps of CRS3W.

3.4 Discussion

3.4.1 Power spectrum

Somatosensory cortex is implicated in the processing of sensory-discriminative aspects of pain or stimulus intensity encoding [65-68]. The strength of activation in this region has been found to increase correspondingly with increasing pain stimulus intensity. Also, it is reported that a number of cortical areas including somatosensory cortex, exhibit spontaneously occurring oscillations in the *mu* frequency (~10 Hz), beta frequency (15–30 Hz), and gamma frequency (30–80 Hz) [69-71]. We found that power in right somatosensory cortex at delta, beta, and gamma-frequency ranges have restored in CRS3W group ($p<0.05$, ANOVA) Fig 3.3.

Of particular interest is the gamma frequency, which has been proposed as a mechanism of temporal integration or "binding" of salient stimulus features across different sensory cortices [72]. It has been observed that changes in gamma are more spatially discrete and somatotopically specific than lower frequency oscillations [73]. Further, stimulus-induced enhancements of electroencephalographic (EEG) power in the gamma frequency range (30–100 Hz) have been consistently observed in multiple sensory modalities [74-77] and hypothesized to play a crucial role in cortical integration and perception [78, 79].

3.4.2 Functional connectivity

The brain is not only defined via the location and magnitude of activation clusters but also through the interaction of neural activity between different areas. After establishing the hypothesis that somatosensory cortex and the gamma band can serve as predictors in spontaneous recovery from depression, we analyzed the EEG data included in this study in the light of functional connectivity at network level. Cross correlation first peak analysis i.e., the correlation value at zero lag, showed increased connectivity mainly between right somatosensory cortex and other regions of primary cortex in the CRS1W group. After three weeks the CRS3W group showed restored connectivity among those regions indicating recovery from depression since there was not any statistical difference between the control and the CRS3W groups' connectivity profile (Fig. 3.4b bottom row). Although all the differences in pairwise channel connectivity were disappeared after three weeks, only somatosensory cortices with frontal regions showed statistically reverse connectivity profile

in the CRS1W group. Which may refer to as that in these specific regions connectivity has restituted marking recovery from depression. Similar were the findings through network analysis.

Of particular interest is the gamma oscillations in the functional network connectivity among somatosensory and frontal cortices. Neurons participating in gamma oscillations synchronize their discharges with very high precision [78].It has been observed that changes in gamma oscillations can give temporal integration, “binding” of salient stimulus features across different sensory cortices, more spatial discreteness, and somatotopical specificity [72, 73].Thus, gamma oscillations facilitate neuronal communication and play a crucial role in cortical integration and perception/cognition [80]. In this study, we can conclude that gamma oscillations in bilinear temporal correlations and multiscale brain network are engaged in spontaneous remission of depression-related behavior.

References

[1] S. M. Banks and R. D. Kerns, "Explaining high rates of depression in chronic pain: A diathesis-stress framework," *Psychological Bulletin*, vol. 119, pp. 95-110, 1996.

[2] S. R. Currie and J. Wang, "Chronic back pain and major depression in the general Canadian population," *Pain*, vol. 107, pp. 54-60, 2004.

[3] S. B. Patten, "Long-term medical conditions and major depression in a Canadian population study at waves 1 and 2," *Journal of Affective Disorders*, vol. 63, pp. 35-41, Mar 2001.

[4] R. J. DeRubeis, G. J. Siegle, and S. D. Hollon, "Cognitive therapy versus medication for depression: treatment outcomes and neural mechanisms," *Nat Rev Neurosci*, vol. 9, pp. 788-96, Oct 2008.

[5] R. C. Kessler, P. Berglund, O. Demler, R. Jin, D. Koretz, K. R. Merikangas, *et al.*, "The epidemiology of major depressive disorder: results from the National Comorbidity Survey Replication (NCS-R)," *JAMA*, vol. 289, pp. 3095-105, Jun 18 2003.

[6] R. C. Kessler, P. Berglund, O. Demler, R. Jin, K. R. Merikangas, and E. E. Walters, "Lifetime prevalence and age-of-onset distributions of DSM-IV disorders in the National Comorbidity Survey Replication," *Arch Gen Psychiatry*, vol. 62, pp. 593-602, Jun 2005.

[7] K. J. Ressler and H. S. Mayberg, "Targeting abnormal neural circuits in mood and anxiety disorders: from the laboratory to the clinic," *Nat Neurosci*, vol. 10, pp. 1116-24, Sep 2007.

[8] M. A. Mayur Pandya, Donald A. Malone Jr., Amit Anand, "Where in the Brain Is Depression?," 2012.

[9] W. C. Drevets, J. L. Price, and M. L. Furey, "Brain structural and functional abnormalities in mood disorders: implications for neurocircuitry models of depression," *Brain Struct Funct*, vol. 213, pp. 93-118, Sep 2008.

[10] R. J. Davidson, D. A. Lewis, L. B. Alloy, D. G. Amaral, G. Bush, J. D. Cohen, *et al.*, "Neural and behavioral substrates of mood and mood regulation," *Biol Psychiatry*, vol. 52, pp. 478-502, Sep 15 2002.

[11] D. A. Seminowicz, H. S. Mayberg, A. R. McIntosh, K. Goldapple, S. Kennedy, Z. Segal, *et al.*, "Limbic-frontal circuitry in major depression: a path modeling metanalysis," *Neuroimage*, vol. 22, pp. 409-18, May 2004.

[12] J. L. Price and W. C. Drevets, "Neurocircuitry of mood disorders," *Neuropsychopharmacology*, vol. 35, pp. 192-216, Jan 2010.

[13] R. L. Buckner, J. Sepulcre, T. Talukdar, F. M. Krienen, H. Liu, T. Hedden, *et al.*, "Cortical hubs revealed by intrinsic functional connectivity: mapping, assessment of stability, and relation to Alzheimer's disease," *J Neurosci*, vol. 29, pp. 1860-73, Feb 11 2009.

[14] V. Jirsa, McIntosh, A.,, " Handbook of brain connectivity. Understanding complex systems.," *Springer*, 2007.

[15] B. Horwitz, "The elusive concept of brain connectivity," *Neuroimage*, vol. 19, pp. 466-70, Jun 2003.

[16] K. J. Friston, "Functional and effective connectivity in neuroimaging: A synthesis," *Hum Brain Mapp*, vol. 2, pp. 56–78, 1994.

[17] P. C. Lauterbur, "Image Formation by Induced Local Interactions - Examples Employing Nuclear Magnetic-Resonance," *Nature*, vol. 242, pp. 190-191, 1973.

[18] M. E. Moseley, Y. Cohen, J. Kucharczyk, J. Mintorovitch, H. S. Asgari, M. F. Wendland, *et al.*, "Diffusion-weighted MR imaging of anisotropic water diffusion in cat central nervous system," *Radiology*, vol. 176, pp. 439-45, Aug 1990.

[19] K. J. Friston, C. D. Frith, P. F. Liddle, and R. S. Frackowiak, "Functional connectivity: the principal-component analysis of large (PET) data sets," *J Cereb Blood Flow Metab*, vol. 13, pp. 5-14, Jan 1993.

[20] A. A. Fingelkurts, A. A. Fingelkurts, and S. Kahkonen, "Functional connectivity in the brain - is it an elusive concept?," *Neuroscience and Biobehavioral Reviews*, vol. 28, pp. 827-836, Jan 2005.

[21] K. J. Friston, "The labile brain. I. Neuronal transients and nonlinear coupling," *Philos Trans R Soc Lond B Biol Sci*, vol. 355, pp. 215-36, Feb 29 2000.

[22] M. Breakspear and J. R. Terry, "Topographic Organization of Nonlinear Interdependence in Multichannel Human EEG," *NeuroImage*, vol. 16, pp. 822-835, 2002.

[23] C. J. Stam, M. Breakspear, A. M. van Cappellen van Walsum, and B. W. van Dijk, "Nonlinear synchronization in EEG and whole-head MEG recordings of healthy subjects," *Hum Brain Mapp*, vol. 19, pp. 63-78, Jun 2003.

[24] Y. Sun, S. Hu, J. Chambers, Y. Zhu, and S. Tong, "Graphic patterns of cortical functional connectivity of depressed patients on the basis of EEG measurements," *Conf Proc IEEE Eng Med Biol Soc*, vol. 2011, pp. 1419-22, 2011.

[25] M. M. Shafi, M. B. Westover, M. D. Fox, and A. Pascual-Leone, "Exploration and modulation of brain network interactions with noninvasive brain stimulation in combination with neuroimaging," *Eur J Neurosci*, vol. 35, pp. 805-25, Mar 2012.

[26] A. F. Leuchter, I. A. Cook, A. M. Hunter, C. Cai, and S. Horvath, "Resting-state quantitative electroencephalography reveals increased neurophysiologic connectivity in depression," *PLoS One,* vol. 7, p. e32508, 2012.

[27] L. Leistritz, T. Weiss, J. Ionov, K. J. Bar, W. H. Miltner, and H. Witte, "Connectivity analysis of somatosensory evoked potentials in patients with major depression. Analysis of connectivity," *Methods Inf Med,* vol. 49, pp. 484-91, 2010.

[28] S. Kito, R. D. Pascual-Marqui, T. Hasegawa, and Y. Koga, "High-frequency Left Prefrontal Transcranial Magnetic Stimulation Modulates Resting EEG Functional Connectivity for Gamma Band Between the Left Dorsolateral Prefrontal Cortex and Precuneus in Depression," *Brain Stimul,* Oct 12 2013.

[29] O. David, D. Cosmelli, and K. J. Friston, "Evaluation of different measures of functional connectivity using a neural mass model," *Neuroimage,* vol. 21, pp. 659-73, Feb 2004.

[30] M. B. Anna Suhhova, Kaire Aadamsoo, Ülle Võhma, Jaanus Lass, Hiie Hinrikus, "EEG Coherence as Measure of Depressive Disorder," *IFMBE Proceedings,* vol. 22, pp. 353-355, 2008.

[31] R.-J. K. Chan-A Park, Seungyeon Kim, Hye-ran Jang, Jeong-Ho Chae, Taemin Kim, Jaeseung Jeong, "Decreased Phase Synchronization of the EEG in Patients with Major Depressive Disorder," 2006.

[32] H. Lee, H. Kang, M. K. Chung, B. N. Kim, and D. S. Lee, "Persistent brain network homology from the perspective of dendrogram," *IEEE Trans Med Imaging,* vol. 31, pp. 2267-77, Dec 2012.

[33] C. J. S. B. C. M. Wijk, and A. Daffertshofer, "Comparing brain networks of different size and connectivity density using graph theory," *PLoS ONE,* vol. 5, 2010.

[34] J. W. Bohland, H. Bokil, C. B. Allen, and P. P. Mitra, "The Brain Atlas Concordance Problem: Quantitative Comparison of Anatomical Parcellations," *Plos One,* vol. 4, Sep 29 2009.

[35] M. Rubinov, S. A. Knock, C. J. Stam, S. Micheloyannis, A. W. F. Harris, L. M. Williams, *et al.*, "Small-World Properties of Nonlinear Brain Activity in Schizophrenia," *Human Brain Mapping,* vol. 30, pp. 403-416, Feb 2009.

[36] L. Ferrarini, I. M. Veer, E. Baerends, M. J. van Tol, R. J. Renken, N. J. A. van der Wee, *et al.*, "Hierarchical Functional Modularity in the Resting-State Human Brain," *Human Brain Mapping,* vol. 30, pp. 2220-2231, Jul 2009.

[37] F. J. van der Staay, S. S. Arndt, and R. E. Nordquist, "Evaluation of animal models of neurobehavioral disorders," *Behav Brain Funct,* vol. 5, p. 11, 2009.

[38] S. L. Gourley, F. J. Wu, and J. R. Taylor, "Corticosterone regulates pERK1/2 map kinase in a chronic depression model," *Ann N Y Acad Sci,* vol. 1148, pp. 509-14, Dec 2008.

[39] D. J. David, B. A. Samuels, Q. Rainer, J. W. Wang, D. Marsteller, I. Mendez, *et al.*, "Neurogenesis-dependent and -independent effects of fluoxetine in an animal model of anxiety/depression," *Neuron,* vol. 62, pp. 479-93, May 28 2009.

[40] S. Jung, J. S. Seo, B. S. Kim, D. Lee, K. H. Jung, K. Chu, *et al.*, "Social deficits in the AY-9944 mouse model of atypical absence epilepsy," *Behav Brain Res,* vol. 236, pp. 23-9, Jan 1 2013.

[41] D. Jeon, S. Kim, M. Chetana, D. Jo, H. E. Ruley, S. Y. Lin, *et al.*, "Observational fear learning involves affective pain system and Cav1.2 Ca2+ channels in ACC," *Nat Neurosci,* vol. 13, pp. 482-8, Apr 2010.

[42] P. a. Franklin, " The Mouse Brain in Stereotaxic Coordinates."

[43] H. J. Caruncho and T. Rivera-Baltanas, "Biomarkers of depression," *Revista De Neurologia,* vol. 50, pp. 470-476, Apr 16 2010.

[44] S. Olbrich, A. Trankner, T. Chittka, U. Hegerl, and P. Schonknecht, "Functional connectivity in major depression: Increased phase synchronization between frontal cortical EEG-source estimates," *Psychiatry Res,* Feb 26 2014.

[45] F. Memoli and G. Sapiro, "A theoretical and computational framework for isometry invariant recognition of point cloud data," *Foundations of Computational Mathematics,* vol. 5, pp. 313-347, Aug 2005.

[46] B. J. He, Snyder, A.Z., Vincent, J.L., Epstein, A., Shulman, G.L. & Corbetta, M. A. van Buchem, J. H. Reiber, S. A. Rombouts, and J.Milles, "Breakdown of functional connectivity in frontoparietal networks underlies behavioral deficits in spatial neglect," *Neuron,* vol. 53, pp. 905-918, 2007.

[47] M. D. Fox, A. Z. Snyder, J. L. Vincent, M. Corbetta, D. C. Van Essen, and M. E. Raichle, "The human brain is intrinsically organized into dynamic, anticorrelated functional networks," *Proceedings of the National Academy of Sciences of the United States of America,* vol. 102, pp. 9673-9678, Jul 5 2005.

[48] R. J. Davidson, D. Pizzagalli, J. B. Nitschke, and K. Putnam, "Depression: perspectives from affective neuroscience," *Annu Rev Psychol,* vol. 53, pp. 545-74, 2002.

[49] R. J. Davidson, "What does the prefrontal cortex "do" in affect: perspectives on frontal EEG asymmetry research," *Biol Psychol,* vol. 67, pp. 219-33, Oct 2004.

[50] A. R. Haig, E. Gordon, V. De Pascalis, R. A. Meares, H. Bahramali, and A. Harris, "Gamma activity in schizophrenia: evidence of impaired network binding?," *Clin Neurophysiol,* vol. 111, pp. 1461-8, Aug 2000.

[51] L. Leistritz, T. Weiss, K. J. Bar, F. De VicoFallani, F. Babiloni, H. Witte, *et al.*, "Network redundancy analysis of effective brain networks: a comparison of healthy controls and patients with major depression," *PLoS One,* vol. 8, p. e60956, 2013.

[52] S. J. Smith, "EEG in neurological conditions other than epilepsy: when does it help, what does it add?," *J Neurol Neurosurg Psychiatry,* vol. 76 Suppl 2, pp. ii8-12, Jun 2005.

[53] N. Razavi, K. Jann, T. Koenig, M. Kottlow, M. Hauf, W. Strik, *et al.*, "Shifted coupling of EEG driving frequencies and FMRI resting state networks in schizophrenia spectrum disorders," *PLoS One,* vol. 8, p. e76604, 2013.

[54] M. F. O'Neil and N. A. Moore, "Animal models of depression: are there any?," *Hum Psychopharmacol,* vol. 18, pp. 239-54, Jun 2003.

[55] R. H. Belmaker and G. Agam, "Major depressive disorder," *N Engl J Med,* vol. 358, pp. 55-68, Jan 3 2008.

[56] A. J. Rush, M. H. Trivedi, S. R. Wisniewski, A. A. Nierenberg, J. W. Stewart, D. Warden, *et al.*, "Acute and longer-term outcomes in depressed outpatients requiring one or several treatment steps: a STAR*D report," *Am J Psychiatry,* vol. 163, pp. 1905-17, Nov 2006.

[57] C. Wijeratne and P. Sachdev, "Treatment-resistant depression: critique of current approaches," *Aust N Z J Psychiatry,* vol. 42, pp. 751-62, Sep 2008.

[58] A. Baskaran, R. Milev, and R. S. McIntyre, "The neurobiology of the EEG biomarker as a predictor of treatment response in depression," *Neuropharmacology,* vol. 63, pp. 507-13, Sep 2012.

[59] E. Driessen and S. D. Hollon, "Cognitive behavioral therapy for mood disorders: efficacy, moderators and mediators," *Psychiatr Clin North Am,* vol. 33, pp. 537-55, Sep 2010.

[60] K. Esposito and P. Goodnick, "Predictors of response in depression," *Psychiatric Clinics of North America,* vol. 26, pp. 353-365, 2003.

[61] K. E. Hamilton and K. S. Dobson, "Cognitive therapy of depression: pretreatment patient predictors of outcome," *Clin Psychol Rev,* vol. 22, pp. 875-93, Jul 2002.

[62] J. L. Voorhees, A. J. Tarr, E. S. Wohleb, J. P. Godbout, X. K. Mo, J. F. Sheridan, *et al.*, "Prolonged Restraint Stress Increases IL-6, Reduces IL-10, and Causes Persistent Depressive-Like Behavior That Is Reversed by Recombinant IL-10," *Plos One,* vol. 8, Mar 8 2013.

[63] R. D. Porsolt, A. Bertin, and M. Jalfre, "Behavioral despair in mice: a primary screening test for antidepressants," *Arch Int Pharmacodyn Ther,* vol. 229, pp. 327-36, Oct 1977.

[64] A. Khalid, B. S. Kim, M. K. Chung, J. C. Ye, and D. Jeon, "Tracing the evolution of multi-scale functional networks in a mouse model of depression using persistent brain network homology," *Neuroimage,* Jul 24 2014.

[65] K. Bornhovd, M. Quante, V. Glauche, B. Bromm, C. Weiller, and C. Buchel, "Painful stimuli evoke different stimulus-response functions in the amygdala, prefrontal, insula and somatosensory cortex: a single-trial fMRI study," *Brain,* vol. 125, pp. 1326-36, Jun 2002.

[66] R. C. Coghill, C. N. Sang, J. H. Maisog, and M. J. Iadarola, "Pain intensity processing within the human brain: A bilateral, distributed mechanism," *Journal of Neurophysiology,* vol. 82, pp. 1934-1943, Oct 1999.

[67] S. Della Penna, K. Torquati, V. Pizzella, C. Babiloni, R. Franciotti, P. M. Rossini, *et al.*, "Temporal dynamics of alpha and beta rhythms in human SI and SII after galvanic median nerve stimulation. A MEG study," *Neuroimage,* vol. 22, pp. 1438-46, Aug 2004.

[68] L. Timmermann, M. Ploner, K. Haucke, F. Schmitz, R. Baltissen, and A. Schnitzler, "Differential coding of pain intensity in the human primary and secondary somatosensory cortex," *J Neurophysiol,* vol. 86, pp. 1499-503, Sep 2001.

[69] S. D. Hall, I. E. Holliday, A. Hillebrand, K. D. Singh, P. L. Furlong, A. Hadjipapas, *et al.*, "The missing link: analogous human and primate cortical gamma oscillations," *Neuroimage,* vol. 26, pp. 13-7, May 15 2005.

[70] G. Pfurtscheller and F. H. Lopes da Silva, "Event-related EEG/MEG synchronization and desynchronization: basic principles," *Clinical Neurophysiology,* vol. 110, pp. 1842-1857, 1999.

[71] A. K. Roopun, S. J. Middleton, M. O. Cunningham, F. E. LeBeau, A. Bibbig, M. A. Whittington, *et al.*, "A beta2-frequency (20-30 Hz) oscillation in nonsynaptic networks of somatosensory cortex," *Proc Natl Acad Sci U S A,* vol. 103, pp. 15646-50, Oct 17 2006.

[72] A. K. Engel and W. Singer, "Temporal binding and the neural correlates of sensory awareness," *Trends Cogn Sci,* vol. 5, pp. 16-25, Jan 1 2001.

[73] N. E. Crone, D. L. Miglioretti, B. Gordon, and R. P. Lesser, "Functional mapping of human sensorimotor cortex with electrocorticographic spectral analysis. II. Event-related synchronization in the gamma band," *Brain,* vol. 121 (Pt 12), pp. 2301-15, Dec 1998.

[74] P. Fries, "Neuronal Gamma-Band Synchronization as a Fundamental Process in Cortical Computation," *Annual Review of Neuroscience,* vol. 32, pp. 209-224, 2009.

[75] C. S. Herrmann and J. Kaiser, "EEG gamma-band responses reflect human behavior: an overview," *Int J Psychophysiol,* vol. 79, pp. 1-2, Jan 2011.

[76] C. M. Karns and R. T. Knight, "Intermodal auditory, visual, and tactile attention modulates early stages of neural processing," *J Cogn Neurosci*, vol. 21, pp. 669-83, Apr 2009.

[77] T. Womelsdorf, P. Fries, P. P. Mitra, and R. Desimone, "Gamma-band synchronization in visual cortex predicts speed of change detection," *Nature,* vol. 439, pp. 733-6, Feb 9 2006.

[78] E. Rodriguez, N. George, J. P. Lachaux, J. Martinerie, B. Renault, and F. J. Varela, "Perception's shadow: long-distance synchronization of human brain activity," *Nature*, vol. 397, pp. 430-3, Feb 4 1999.

[79] C. Tallon-Baudry, O. Bertrand, C. Delpuech, and J. Permier, "Oscillatory gamma-band (30-70 Hz) activity induced by a visual search task in humans," *J Neurosci,* vol. 17, pp. 722-34, Jan 15 1997.

[80] E. Basar, "A review of gamma oscillations in healthy subjects and in cognitive impairment," *Int J Psychophysiol,* vol. 90, pp. 99-117, Nov 2013.

Summary

Tracing the evolution of multiscale functional network and prediction of spontaneous remission in the EEG of depression mouse models using persistent homology

다양한 뇌의 질병 또는 우울증과 같은 질환은 뇌의 신경망 연결에 비정상적인 기능을 한다고 알려져 있다. 다양한 우울증 증상의 징후를 관찰하기 위해, 교차 상관 관계 및 일관성 측정 등의 커플링 분석을 위한 기존의 두 변수의 측정을 기반의 뇌의 기능성 연결성 연구와는 다른 방법을 설명하고자 한다. 우리는 데이터에 존재하는 최적의 정보들의 사용을 보장하면서 신경망 단계의 우울증 마우스 모델 EEG 를 관찰함으로써 좀 더 포괄적인 방법을 채택하였다. 신경망 진화의 기하학적인 정보 사용을 위해, 우리는 지속적 유사성 (persistent homology) 신경망의 분석을 우울증 마우스 모델의 EEG 신호에 적용하였다. EEG 신호는 8 개의 서로 다른 피질 영역 (정면, 체성 감각, 두정엽, 각 반구의 시각 피질)에서 얻을 수 있었다. 지속적 유사성 연구로부터 정상군 및 우울증 마우스 모델에서 기능성 연결이 상당히 다른 것을 발견하였다. 이는 일반적인 교차 상관 관계 및 일관성 측정 등의 커필링 측정에서는 발견되지 않았다. 우울증 마우스 모델에서는 좀 더 작은 영역에 신경 연결이 모여 있었고 정상군에 비해 전체적인 연결성이 감소하는 것을 확인할 수 있었다. 특히, 체성 감감과 두정엽 피질은 우울증 모델에서 다소 연결성이 떨어졌다. 또한, 우울증 모델에서는 특히 정면 및 체성 감각 피질 사이 피질 영역간에 정상군과 비교했을 때 다른 연결성을 보여주었다. 본 연구는 지속적 유사성이 뇌의 연결을 분석함에 있어서 매우 유용한 것을 확인 하였고 결과적으로 우울증에 걸린 동물의 뇌는 좀

더 작은 영역에 신경이 모여서 동작하고 전체적인 신경망은 감소하는 것을 보여주었다. 이런 결과를 토대로 우울증으로 인한 비정상적 신경망 분류에 도움이 될 것으로 기대한다. 더 나아가 우울증 등 많은 질병이 치료 시간에 구애 받지 않고 스스로 제어할 수 있게 될 것으로 기대하고 자연 치유의 관점에서 변화가 예상된다. 최근 우울증에서 원상 복구 요인들을 관찰하고 정량적 EEG 분석을 통해 예측이 적합한지 확인하고 있다. 이번 연구에서, 우리는 만성 스트레스를 가한 마우스 모델에서부터 EEG 경보 상태 데이터를 측정하였다. 우울증에서부터 자연 치유가 되는 3 주 후에 EEG 측정을 다시 하였다. 우리는 만성스트레스 모델이 정상군과 비교했을 때 3 주후에 피질의 스펙트럼 신호가 복원 되었음을 확인하였다. 정면 피질과 체성 감각 피질은 기본적으로 자연 복원을 보여주었다. 신경망 수준의 기능성 연결은 지속적 뇌 연결의 유사성과 또 다른 그래프 이론 측정과 함께 분석 되었다. 3 주후에 연결성 레벨에서 시간 방향 진동의 변화된 기능성은 주로 감마 주파수 영역 (31-80 Hz)에서 체성 감각 피질을 포함하는 정상군 결과와 유사한 것을 확인할 수 있었고 감마 영역의 변화를 통해 우울증에 영향을 받은 뇌의 회복을 예측할 수 있을 것으로 기대한다.